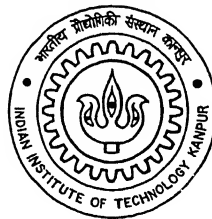# Drawbead Analysis for Axisymmetric Hemispherical Bottom Components

A Thesis Submitted for
partial fulfillment of Requirements for the Degree of
Master of Technology

by

Danendra S. Bhatnagar

to the

**DEPARTMENT OF MECHANICAL ENGINEERING
INDIAN INSTITUTE OF TECHNOLOGY
KANPUR**

CERTIFICATE
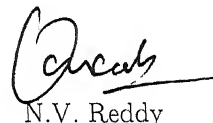
It is certified that the work contained in the thesis entitled "*Drawbead Analysis for Axisymmetric Hemispherical Bottom Components*", by Mr. Danendra S. Bhatnagar, has been carried out under my supervision and that this work has not been submitted elsewhere for a degree.

N.V. Reddy

Department of Mechanical Engineering

Indian Institute of Technology Kanpur

June, 2005
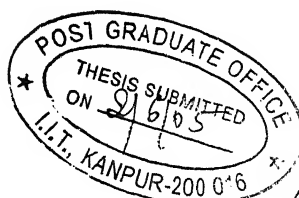
Acknowledgements

I am highly thankful to my thesis supervisor Dr. N. Venkata Reddy for his excellent guidance, constant encouragement and the enormous confidence he had in me. Without his motivating talks and support during my tough times, this work would not have been possible.

I thank my friends Nagarajan, Deep, Kalyan, Vinod, Sanjeev, Seshank, Ganesh, Navin, Ritesh, and Sandeep for the excellent time I had with them for the last two years. I am grateful to my seniors Anupam, Deepak, Sachin, Sunil, Manas, Prince, Pritam, Sudhish, Kisun for their valuable suggestions and help.

I am indebted to my parents and sisters for their support and encouragement.

At last, but not the least, I am thankful to everyone who helped me directly or indirectly to complete this work.

<div align="right">Danendra S. Bhatnagar</div>

Abstract

Restriction of the flow of material into the die cavity is the major requirement in the stretch forming for producing wrinkle free hemispherical cups. This is achieved by using blankholder with the drawbeads. Drawbeads are the added projection on the blank holder surface which fits into a groove on the external part of the die surface. The drawbead increases the restraining force against the flow of material in the flange region due to the bending and unbending of the sheet over the drawbead and groove shoulders. The restraining force due to improper design of the drawbead can make the sheet stretch or excessively draw which will result in the defective products. Hence its imperative that the drawbead should be designed properly keeping in view the specific requirement of the process. Restraining force depends mainly on the geometrical parameters of drawbead. In the present work an attempt has been made to study the effect of geometrical parameters of drawbead on the restraining force in the axisymmetric hemispherical punch stretching process. A method has been devised for the analysis of stretching of circular blanks with hemispherical punch based on the principle of force equilibrium and total strain theory. The sheet is assumed to be deformed under the membrane stresses only. The stresses, strain, punch load vs travel relationship and the deformed configuration of the sheet are predicted using the developed model. The results predicted by the present method are compared with the available finite element method[1](source [2]), energy minimization method[2] and experimental results[1](source[2]) available in literature and are found to be in good agreement. The predicted limiting dome height is found to be in reasonably good agreement with the reported results[3] having a maximum error of $\pm 9\%$. The effect of process parameters namely friction condition, strain hardening exponent and normal anisotropy on the process mechanics are studied and it is observed that a larger value of strain hardening exponent, a lower value of normal anisotropy and a lower value of friction coefficient results in more uniform strain distribution in the deformed region and a larger value of limiting dome height.

An analytical model based on the slab method is proposed for analyzing the flow of the metal over the drawbead. The developed model is used to find out the restraining force at the die opening when the drawbead is locked with the groove shoulders on the die surface. The effect of geometric parameters namely drawbead height, radius of drawbead and drawbead groove shoulder and clearance between the drawbead and drawbead

groove shoulder on the restraining force are studied. It has been observed that a larger value of drawbead height, a smaller values of radius of drawbead and groove shoulder and a smaller value of clearance give more restraining force which leads to increased restriction of the flow of material into the die opening.

Contents

List of Figures

Nomenclature

a	Radius of the clamped boundary
b	Radial distance between the center of drawbead and drawbead groove shoulder
c	Clearance between the drawbead and drawbead groove shoulder
H	Punch Travel
H_d	Drawbead Height
K	Strength constant
L_i	Length of inner flat flange
L_o	Length of outer flat flange
n	Strain hardening exponent
P	Punch load
p	Punch pressure
p_{bh}	Blank holding pressure
r, θ, z	Cylindrical co-ordinate system
$\bar{R}$	Normal anisotropy ratio
R_0	Initial blank radius
R_d	Radius of drawbead
R_g	Radius of drawbead groove shoulder
R_p	Radius of hemispherical punch
r_0	Current outer radius of the sheet
s	Initial radius on the undeformed blank
t	Current sheet thickness
t_c	Current sheet thickness at contact point of the sheet with the punch
t_0	Initial sheet thickness
$\bar{\epsilon}$	Equivalent strain
$\epsilon_r, \epsilon_\theta, \epsilon_t$	Strain in radial, circumferential and thickness direction
θ_d	Half of the angle over which the sheet is in contact with the drawbead.
μ	Coefficient of friction
ρ_ϕ	Principal radius of curvature in meridian direction
ρ_θ	Principal radius of curvature in circumferential direction
$\bar{\sigma}$	Equivalent stress

$\sigma_\phi, \sigma_\theta, \sigma_t$	Stress in meridian, circumferential and thickness direction
σ_b	Bending stess
σ_{t_1}	Normal external stress acting on the inner surface
σ_{t_2}	Normal external stress acting on the outer surface
τ_1	Frictional stress acting on the inner surface
τ_2	Frictional stress acting on the outer surface
ϕ	Angle made by the normal at a point with the line parallel to shell axis
ϕ_c	Angle made by the normal at the contact point (of sheet and punch) with the line parallel to shell axis

Chapter 1

Introduction and Literature Review

1.1   Introduction

Stretch forming is one of the important sheet metal forming processes. In this forming process, the edge of the sheet is clamped by a die, and then a punch head is pushed into the workpiece to produce the desired shape. It is also commonly used in conjunction with the deep drawing process. When the drawn part being produced has a bottom which is not flat, stretch forming is implemented. Hemispherical bottom cups, as shown in fig.1.1 are the most common shape. No female die is used in stretch forming. The initial stages of drawing produces the bottom of the cup by stretching the blank over the tip of punch.
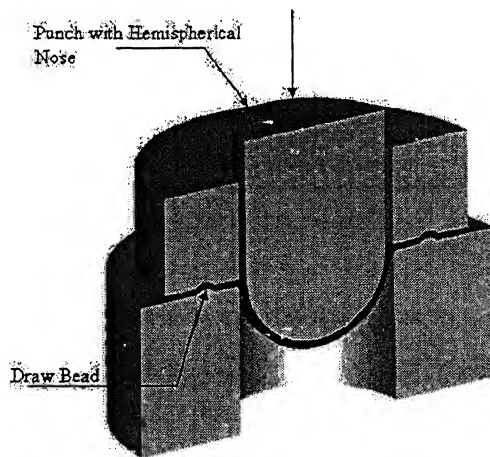
Figure 1.1: *Typical Layout for Hemispherical Punch Stretching*

A high blank holder force and friction forces are required for stretch forming in order to impede the blank from flowing over the die radii until the stretch form is nearly complete. Severe wrinkling or puckering will occur at the cup bottom if the flow is not restricted.

1

The method employed to retard the flow is the use of drawbeads. These drawbeads, as shown in fig.1.1 produce a bend/straighten process which restrict the flow of the material into the die opening. This flow restriction of the material into the die converts the state of stress from tensile-compressive to biaxial tensile stresses in die opening region which produce the required stretching around the punch profile.

Drawbeads are also extensively used in the stamping of automobile body parts and other irregular components. These parts are usually composed of complex free surfaces. Since the geometrical surfaces are non-symmetric, sheet material will not flow uniformly during the drawing process. Due to this some areas have the tendency of fracture with much reduction of thickness and some areas tend to wrinkle after a product is formed. Therefore, to achieve more uniform flow of metal into the die, drawbeads are used in the flange region to produce defect free products.
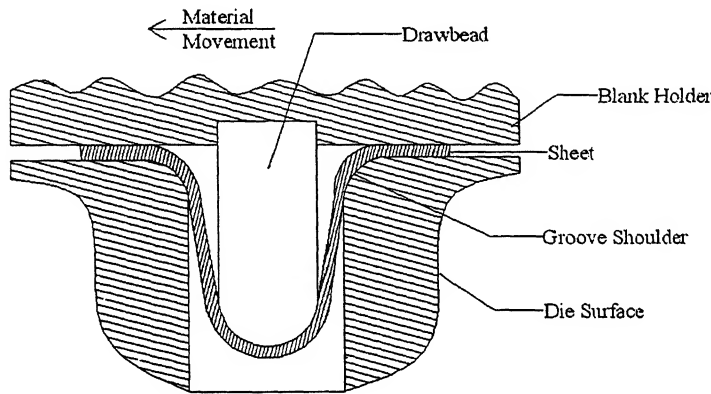
Figure 1.2: *A circular drawbead with rectangular groove[4]*
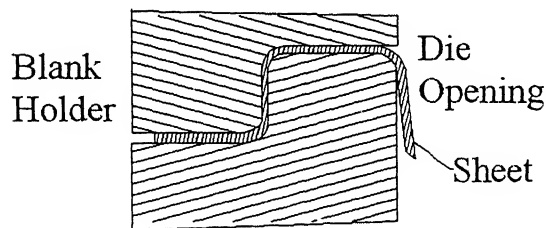
Figure 1.3: *The drawbead placed inside the blankholder region or on the edge of die(die edge)[4]*

Although drawbead of various geometries have been reported in the literature, the more commonly used configurations of the drawbead[4] are shown in figs.1.2-1.4.

Figure1.2 shows the most commonly used drawbead in the drawing process. It consists of semi-cylindrical drawbead on the blank holder surface which fits into the quarter-cylindrical groove shoulders of the square grove on the external part of the die surface.

2
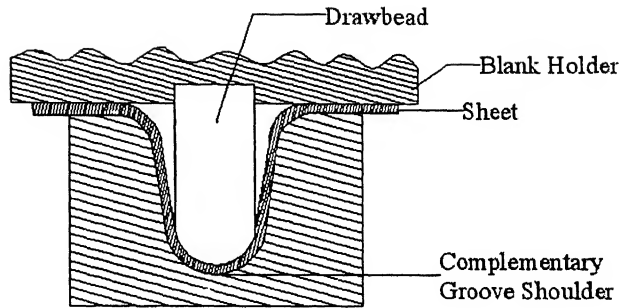
Figure 1.4: *The groove of the complimentary shape as the bead[4]*

In the another configuaration, the drawbead can be placed inside the blank holder or on the edge of die (edge bead) as shown in fig.1.3. The advantage of the edge bead is that the blank size can be reduced and considerable sheet material may be saved. However, the clearance in this type is usually very small and the effective bead radius of the sheet equals the tool radius. Due to these facts, the sheet is forced to confirm to the bead contour, and a maximum force is generated for a given tool radii. In addition, a possibility of fatigue fracture of the sheet metal at the die edge may also appear when the edge bead is placed too close to the die shoulder.

Another configuaration of drawbead is shown in fig1.4. A groove having the complimentary form of the drawbead presses the sheet tightly to the bead. The restraining force increases due to additional friction between the sheet and the groove. When the sheet edge passes the bead, this type of groove prevents the wrinkling to occur. However the machining of the groove is time consuming and the adjustment of the clearance between the bead and the groove is difficult.

Considerable tryouts by trial and error becomes inevitable for the proper drawbead design for the process since the number of variables such as tool geometry, friction, blankholder force affect the flow of sheet metal in the die. To reduce the try outs which consume a great deal of time, it is very important for a die designer to make a precise decision about the fitness of the drawbead used to control the flow of the sheet metal into the die cavity in early design stages. If the design of drawbeads is not suitable, it makes the sheet stretch or draw excessively because the improper restraining force acts on the sheet. Therefore, it becomes important to systematically analyze the metal flow from the drawbead so that the tedious tryouts can be reduced.

1.2 Literature review

In this section an extensive literature review for both the hemispherical punch stretching as well as the drawbead analysis are presented. First the literature review related to stretching is presented and is followed by the literature review of the drawbead analysis.

Stretching

The problem of punch stretching has been extensively studied both theoretically and experimentally in the past. It is not possible to cover the full exhaustive literature in this area, however the important works which are referred and available to the author are presented in this section. First the analytical and semi-analytical approaches that are made to analyze the problem are presented which is followed by some finite element approaches that are made towards analyzing the stretching process.

One of the first numerical analysis for the hemispherical punch stretching of the circular blanks was done by Woo[5] using incremental theory of plasticity. He developed the general numerical solution for the axisymmetric forming problems. He considered material as an isotropic and used a successive approximation technique for calculating the developed stress and strains in the sheet during stretching of the sheet. The deformation was assumed to be in plane stress condition. He used a geometrical approximation for relating the circumferential and tangential strains by calculating the area of the element in the deformed region as a frustum of cone. It was reported that the non-convergence of static equilibrium equation in the numerical solution corresponds to point of instability in the cup.

Chakrabarty[6] presented the only available complete analytical solution for the hemispherical punch stretching of circular blanks. The problem is analyzed under the membrane stresses alone . The material was assumed to be isotropic and the punch head was assumed to be well lubricated so that the friction can be neglected. Biaxial state of stress was assumed throughout the deformation region, so the solution was valid for the materials which strain hardens according to the law

$$\sigma = Y e^{\epsilon}$$

where Y is the initial yield stress and ϵ is the thickness strain in the sheet. He also reported that the punch load does not have a stationary value in the interval $0 < \phi_c < \frac{\pi}{2}$, where ϕ_c is the angle made between the axis of the shell and the normal to the hemispherical surface at the contact boundary .

Kaftanoglu and Alexander[7] carried out theoretical and experimental work on the axisymmetric stretch forming of circular blanks over the hemispherical and ellipsoidal

punches. They considered the material to be normal anisotropic and the effect of thickness stress is taken into account. They used the strain compatibility equation for relating the principal strains in the numerical analysis. They reported that the non-convergence of static equilibrium equation in the numerical solution corresponds to the limiting stage in the deformation of material at which the strain at a point cannot be transmitted to the neighboring point. They defined this condition as strain propagation instability. They reported that the onset of fracture is very closely predicted by the strain propagation instability and no further numerical solution can be obtained after it was reached. It was also reported that the friction is most important variable in stretch forming. They concluded by the experimental investigation that the friction condition changes with the deformation of sheet in the stretch forming.

Lee and Yang[2] used the energy method to analyze the hemispherical stretching problem of the clamped circular sheets. They assumed negligible thickness stress and the problem is analyzed under membrane stresses only. Normal anisotropy of the sheet material and friction among the sheet-tool interface was considered in the analysis. In the analysis, the deformation region is divided into the supported and unsupported zones. The geometry and the kinematically admissible velocity fields were constructed for the corresponding zones in terms of some unknown parameters. The optimum values of these parameters were then determined by minimizing the total deformation energy using Fletcher-Powell optimization method. The die profile radius is ignored in the analysis. The results predicted were in good agreement with the results of the finite element method and the experimental data[1](source[2])

D. Banabic[8] studied the effect of punch vibration in the hemispherical punch stretching. He reported that the friction between sheet-tool interface varies with the vibration of punch. He modelled friction coefficient as a function of punch vibration and predicted stress and strains using the analysis presented by Woo[5]. He reported that the increase of the vibration frequency up to the limit of 100Hz leads to the improvement of lubricating conditions. On account of this, he reported that increase of the vibration frequency moves the fracture position of the sheet towards the pole.

Some of the important finite element approches that are made to analyze the hemispherical punch stretching process are presented as below

Wifi[9] presented an incremental variational method to analyze axisymmetric elastic plastic solids undergoing large deformation. The method was applied to solve the problem of stretch forming as well as the complete deep drawing of a circular blank using a hemispherical punch. He considered the bending effect over the die profile. Friction at the tooling/workpiece, which is of primary significance, was not taken into account in the analysis. For stretch forming, the outer periphery of the sheet was assumed to be fixed at die opening. The localization of strain was reported at the high stages of punch travels in stretch forming. The calculations at this stage was stopped assuming that the further advance of punch will cause a failure of sheet. The cup height at this stage was

taken as a measure of metal formability.

Kim et al.[10] analyzed the hemispherical stretching using rigid-plastic finite element method based on variational formulation for the problem. Plane stress condition was assumed in the deformation region. The effect of interface friction and the influence of modelling of constitutive relations on the detailed mechanics were examined. It was reported that increase in friction reduces the thinning in contact region while more thinning is observed in non-contact regions. This increases the non-uniformity in the distribution of thickness strain i.e. the peak vale of the strain shifts to edge of hemispherical dome with the increasing friction.

Hsu and Chu[11] developed an elastic-plastic finite element method for the analysis of axisymmetric metal forming processes such as punch stretching, deep drawing and hydro forming. The variational formulation for the problem is developed under the plane stress condition. The sheet is assumed to satisfy a rate sensitive, Mises-type flow rule which takes into account work hardening and anisotropy. The frictional stress at the tool-sheet interface is calculated from the Coulomb frictional law.

Yoshida et al.[12] developed the elastic-plastic finite element method and used the forming limit theory to determine the limiting dome height in the hemispherical stretching of rectangular blanks. The predicted results were validated by the related experimental work and were in good agreement. They reported the effect of material properties such as strain hardening exponent and normal anisotropy on the limiting dome height and strain distribution in the deformed region.

Yang and Hsu[3] extended the work of Yoshida et al.[12] for the hemispherical punch stretching of the circular blanks. The effect of material properties such as strain hardening exponent and normal anisotropy on the strain distribution and limiting dome height were presented.

Drawbead Analysis

The analysis of the sheet metal flowing over the drawbead has been extensively studied by various researchers in the past. Most of these analysis are for the straight drawbeads that are used in stamping analysis. Similar to the stretching the analytical approaches are mentioned first which is followed by the finite element approaches.

Nine[13](source Chen and Tszeng[14]) has carried out the first systematic study of the flow of metal through the straight semi-cylindrical drawbeads. He designed a drawbead simulator and conducted a series of experiments on various steels and aluminium alloys. He also replaced the shoulders and bead of the drawbead with rollers to isolate the bending deformation component from the friction component. He reported that Coulomb friction holds for most steels but breaks down for some material, such as Al 2036-T4 when drawn over a very small radius drawbead.

Chen and Tszeng[14] analyzed the flow of metal over the straight semi-cylindrical draw-bead in the stamping process. They considered that the sheet does not remain in contact with the bottom of groove in the locked position. They developed a theoretical model based on the virtual work principle for calculating the drawbead restraining force. The process is assumed to be a steady process i.e. the restraining force was assumed to reach the steady state value once the first material point completes its travel across the draw-bead. The deformation was assumed to be in plane-strain condition along the width direction and thickness stress was neglected in the comparison of bending stresses developed in the sheet. The variation of thickness along the drawbead was also neglected in the analysis. The plane section is assumed to remain plane after the bending and the Bauschinger effect due to cyclic bending and unbending is ignored.

Samuel[4] experimentally and theoretically investigated the metal flow from the draw-bead used in the stamping problem. He considered that the sheet does not remain in contact with the bottom of groove in the locked position. He assumed the strain along the width direction is negligible. The thickness stress was also assumed to be negligible during the deformation. He suggested that the entire restraining force of the drawbead is due to the work done in the three bending and unbending sequences and the frictional forces along contact of sheet with the bead and groove shoulders. The bending forces are calculated on the basis of equilibrium of forces. Belt-pulley analogy is used for calculating the frictional forces over the drawbead and groove shoulder regions. The influence of cyclic bending on the constitutive law was taken into consideration in their model. He also carried out experiments to analyze the flow of sheet over two different drawbead geometries namely semi circular male bead with round and square female bead. He reported that for square female draw bead restraining force is higher than those for the rounded female bead because geometry of the square bead involves relatively sharp corners in the female bead which results in concentrated contact area over an even smaller region than the round female bead.

Weidemann[15](source Shuhui et al.[16]) proposed a simple analytical model for calculating the draw bead restraining force for the straight drawbead of circular cross-section. Their model consider the restraining force from bending and friction force only and is given by

$$DBRF = \left[\left(F_{c1} + F_1 e^{\mu\theta} + F_2 + F_3 \right) e^{2\mu\theta} + F_4 + F_5 \right] e^{\mu\theta} + F_6$$

where F_{c1} is the friction force acting on the outer flange region and F_i are bending/unbending force acting on each bending/unbending point over the drawbead region. The strain in the width direction is assumed to be zero. The thickness stress is assumed to be negligible and material was assumed to be isotropic.

Sanchez and Weinmann[17] presented an iterative approach based on finite difference method for determining the forces and bending moment required to form sheet metal subject to plane strain conditions. They assumed the plane stress state across the thickness. The method can be applied to any arbitrary geometry and cyclic bending effects

were also included in the method.

Many finite element approaches has been used by the different authors for analyzing the flow of metal over the drawbead. Some of them are presented as follows

Triantafyllidis et al.[18] developed a one dimensional elastic-plastic finite element method for analyzing the straight drawbeads of circular and rectangular sections. The strain in the width direction is assumed to be negligible. The problem is also assumed be in plane stress state across the thickness. They reported that deep, narrow beads are seen to provide the greatest restraining force during the pulling phase of deformation, but also have the greatest risk of sheet failure during the locking phase. Wide, shallow beads produce little risk of tearing during locking, since strains across the sheet are lower and more uniform, and also allow material to pull through more easily as the panel is formed. Yang et al.[19] carried out a 2D elastic plastic FE analysis for the drawing process using a straight drawbead of circular and rectangular cross section. The metal flow is assumed to be in plane strain condition. They reported that draw bead restraining force increases with the decrease in drawbead height and with the decrease of the radius of drawbead and drawbead groove shoulder.

Meinders et al.[20] proposed an equivalent drawbead model finite element code for the analysis of complete stamping process. They reported that since the size of the draw-beads is usually very small compared with the remaining portion of the die surface, the sheet metal which is pulled through the drawbeads during drawing must be modelled by very small elements to reflect the effect of bending deformation of the sheet metal around the drawbeads. A finite element model with such element proves to be uneconomical in terms of the computational time. Hence an equivalent drawbead model was used to replace the full scale physical modelling of the drawbead in the finite element simulation of a sheet metal forming operation to save computational time. In the equivalent drawbead model, the actual drawbead is replaced by its projection on the blank holder surface i.e. a flat surface which has the same width as the actual drawbead, and a regular mesh is constructed for the flat surface. They calculated the restraining force and strain distribution developed due to actual drawbead by the 2D plain strain FE analysis and these values were assigned distributively to the nodes in the regular mesh of the equivalent drawbead model. They then used this developed equivalent drawbead model for the finite element analysis of strip test and the deep drawing of a rectangular product.

Keum et al.[21] developed an expert drawbead model for the straight circular and stepped drawbead similar to the model proposed by Weidemann[15] (source [16]). The drawbead restraining force and bead exit thinning calculated from the expert model are used as a boundary condition of the node nearest to the drawbead exit position. They used the following model to regard the drawbead as a boundary condition

$$FI < DBRF \text{(stretching)} \text{ and } FI = DBRF \text{(draw-in)}$$

where FI is the internal force when the sheet passes through the drawbead at the beginning of stamping.

Li Shuhui et al.[16] developed an equivalent drawbead model by including normal anisotropy ratio in the model developed by Weidemann[15](source[16]) . The three dimensional analysis of the deep drawing process was performed to determine the optimum distribution of drawbead restraining force for the stamping of the joint panel of gate pillar. The optimum design of the drawbead geometry was executed by means of nonlinear constraint optimization with the improved equivalent drawbead model. The obtained drawbead geometry parameters are found to produce the defect free production panels. Cao and Teodosiu[22] carried out a finite element modelling of the drawbeads, by taking into account the whole deep drawing process in the case of axisymmetric deformation. They reported that shrinking and thickening of flange induce non-stationary flow of metal through the drawbead, which are absent in plane-drawing. Coulomb friction with sticking/gliding condition is assumed between the sheet and tools (blankholder, punch and die). They reported that after the locking phase the restraining force first decreases and then sharply increases to a level from which on a more gradually increase is produced by the thickening of the flange. Finally, when the flange rim begins to move through the bead a lower quasistationary level is being reached by the restraining force.

1.3 Scope and the objective of present work

From the critical review of the literature, it can be clearly noticed that although an extensive work has already been done for designing a drawbead for the stamping process, no attempt has been made for the design of drawbead for the process of hemispherical stretching.

To design a proper drawbead for the process of hemispherical stretching, it becomes imperative to have the knowledge of stresses and strains which will get developed due to stretching of the sheet. It can be seen from the literature review that the process of hemispherical cup stretching has been well investigated experimentally as well as theoretically. Still due to high complexity of the problem due to moving contact boundary, the numbers of attempts in the semi-analytic method are quite less in comparison to finite-element analysis. The numerical approaches made to analyze the hemispherical stretching process are that of Woo[5], Kaftanoglu and Alexander[7]. These numerical solutions are based on incremental theory of deformation and are reported to take more time computationally. The finite element approaches are also reported to be computationally uneconomic but are more accurate than the analytical approaches.

Crtitical review of the literature reveals that an analysis of the flow of metal over the straight drawbeads is well attempted in the past. These drawbeads are mostly used in the stamping and deep drawing of rectangular blanks where the width is assumed to remain

constant during the flow of metal over the drawbead. Therefore in these attempts the sheet metal is assumed to deform with negligible strain along the width direction(plane strain condition). However no analytical attempt is known to author for the drawbead analysis in the axisymmetric sheet metal forming process which is characterized by the flange shrinking.

The objective of this work is to investigate the effect of various drawbead geometry parameters for providing the effective restraining force in the axisymmetric hemispherical punch stretching process. The problem of hemispherical stretching is analyzed by the developed method based on the principle of force equilibrium and total deformation theory. In this approach, all the stresses and strain developed in the sheet at a particular punch travel are calculated by taking into consideration the current configuration only. The method is found to give a fast solution and the predicted results are found to be in reasonably good agreement with the results reported in literature.

A simple analyitical approach based on slab method is proposed to study the metal flow through drawbead with circular cross section for axisymmetric hemispherical punch stretching process. The effect of drawbead geometry on the restraining stress developed at the die opening is presented.

1.4   Organization of thesis

Brief introduction of the hemispherical stretching process and the drawbeads that are used in sheet metal forming process is given in this chapter which is followed by the related literature survey. Scope and objective of the present work is also defined in this chapter. The organization of the thesis report is as follows:

Chapter 2 presents the mathematical formulation for hemispherical punch stretching of the circular blanks is which is followed by the mathematical formulation for the drawbead analysis.

Chapter 3 presents the validation of the predicted results obtained from the stretching analysis with the results reported in literature. This is followed by the parametric study in stretching. Lastly, the study of effect of drawbead geometry parameters on the restraining force is presented.

Chapter 4 concludes the report with the scope of future work.

Chapter 2

Mathematical Formulation

2.0.1 Introduction

Main aim of the theoretical and applied research in the metal forming is to find out the optimum ways of producing defect free products. The optimization criterion may vary, depending on product requirements, but establishing an appropriate criterion requires thorough understanding of the forming processes. In any metal forming process, proper design and control requires, among the other things, the determination of deformation mechanics involved in the process. Without the knowledge of the influences of variables such as friction conditions, material properties, and workpiece geometry on the process mechanics, it will not be possible to design the equipment adequately, or to predict and prevent the occurrence of defects. Thus, the mathematical modelling for the process simulation has become a major tool in modern metal forming technology.

In this chapter, a method based on force equilibrium and total deformation theory is presented for calculating the stresses and strains and deformed configuration of the circular sheet when it is stretched by the hemispherical punch. The formulation for the same is presented in section2.0.2. The restraining force developed at the die opening after the locking of the drawbead with the groove shoulders on the die surface is presented in section2.0.3.

2.0.2 Formulation for the stretching analysis

Assumptions

In metal forming processes the geometry of forming tools, work hardening, friction force, etc., influence the forming load and the flow characteristics in a complicated manner. Assumptions therefore, become necessary to set up an simple analytical model for the

analysis. In the present work, following assumptions are employed for the analysis of hemispherical cup stretching.

- The material properties are assumed to be rotationally symmetric i.e. there is a planar isotropy and normal anisotropy. The normal anisotropy value can be defined as

$$\bar{R} = \frac{R_{0^\circ} + 2R_{45^\circ} + R_{90^\circ}}{4} \tag{2.1}$$

where R_{0°, R_{45° and R_{90_o} are the values of anisotropy at 0°, 45° and 90° to the rolling directions respectively.

- Process is assumed to be quasi-static.

- Ratio of the punch radius to the material thickness is large in the hemispherical stretching and the material is stressed well into the plastic region under severe biaxial tension. Hence the bending stresses which are caused by the instantaneous bending of the sheet metal onto the punch surface at early stages of the deformation are small and are therefore ignored in comparison to the membrane stresses in the meridian and circumferential directions.

- The pressure applied by the punch on the sheet is much less than the yield stress and it is assumed that the stress in the thickness direction is negligible in comparison to other principal stresses (plane stress condition).

- Die profile radius has been neglected in the analysis and therefore the sheet supported by the die profile is considered as free region.

- Material is assumed to yield according to Hill's anisotropic criterion.

- The strain hardening characteristics of sheet metal is assumed to follow the form

$$\bar{\sigma} = K(\bar{\epsilon})^n \tag{2.2}$$

where $\bar{\sigma}$ is the equivalent stress, $\bar{\epsilon}$ is the equivalent strain, n is the strain hardening exponent and K is a material constant.

Hill's Anisotropic Yield Criterion

Hill's anisotropic yield criterion[Hill,1950] for total deformation theory is given as[23]

$$\bar{\sigma} = \frac{1}{\sqrt{1 + \bar{R}}}[(\sigma_\theta - \sigma_t)^2 + (\sigma_\phi - \sigma_t)^2 + (\sigma_\phi - \sigma_\theta)^2]^{\frac{1}{2}} \tag{2.3}$$

$$\bar{\epsilon} = \frac{\sqrt{1 + \bar{R}}}{1 + 2\bar{R}}[(\epsilon_\theta - \bar{R}\epsilon_t)^2 + (\epsilon_\phi - \bar{R}\epsilon_t)^2 + \bar{R}(\epsilon_\phi - \epsilon_\theta)^2]^{\frac{1}{2}} \tag{2.4}$$

$$\frac{\epsilon_\phi}{\bar{R}(\sigma_\phi - \sigma_\theta) + (\sigma_\phi - \sigma_t)} = \frac{\epsilon_\theta}{\bar{R}(\sigma_\theta - \sigma_\phi) + (\sigma_\theta - \sigma_t)} = \frac{\epsilon_t}{(\sigma_t - \sigma_\theta) + (\sigma_t - \sigma_\phi)} = \frac{\bar{\epsilon}}{(1 + \bar{R})\bar{\sigma}}$$
$$(2.5)$$

where σ_ϕ, σ_θ, and σ_t are the stresses and ϵ_ϕ, ϵ_θ and ϵ_t are the strains in the meridian, circumferential and thickness directions respectively.

Shell Geometry

An axisymmetric shell, or surface of revolution is shown in Fig2.1(a). A point on the surface, P, can be described in terms of the cylindrical coordinates r, θ, z as shown in the given Fig.2.1(a). The curve generating the shell, C, is illustrated in Fig2.1(b). The

(a) *Surface of revolution*   (b) *Generating Curve*
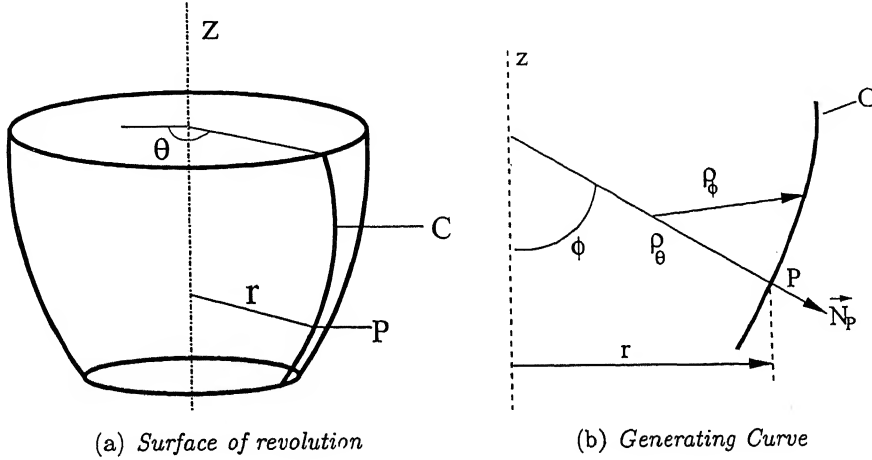
Figure 2.1: *Shell Geometry*

outward normal to the curve (and the surface) at P is $\vec{N_P}$. This makes an angle ϕ with the axis. Circumferential and meridian radii of curvature are the two principal radii of curvature as shown in the Fig.2.1(b). The arc length of the element along the meridian
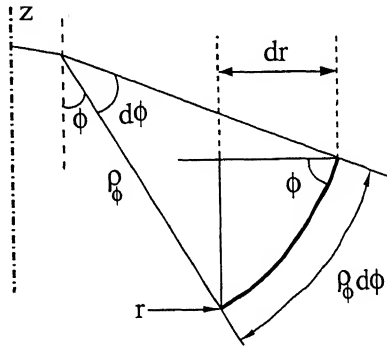
Figure 2.2: *An meridian element on a shell*

is $ds = \rho d\phi$ and from Figs.2.1(b) and 2.2, following geometric relations can be obtained for the principal radii of curvature and are given as

13

$$\rho_\phi = \frac{\partial r}{\partial \phi} \sec \phi \qquad (2.6)$$

$$\rho_\theta = r cosec\phi \qquad (2.7)$$

Equilibrium Equations
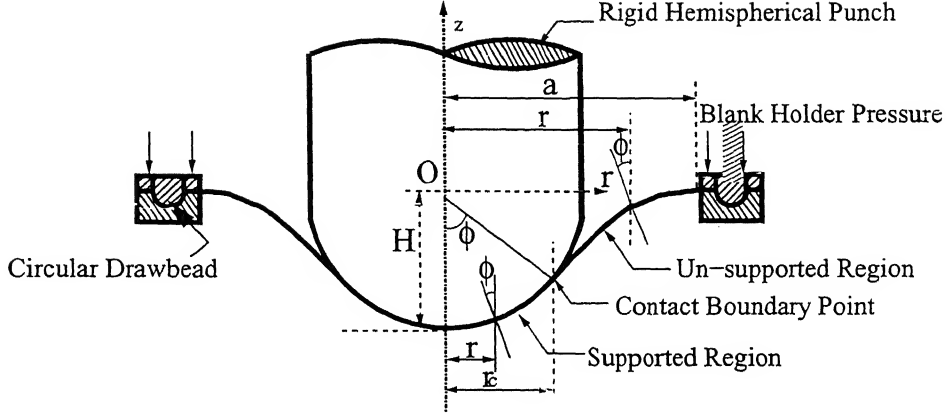
Figure 2.3: *Schematic View of Hemispherical Stretching Process*

Consider a clamped thin circular sheet subjected to the lateral loading by a rigid hemispherical punch as shown in the Fig2.3. The principal coordinates of deformation are assumed to be along circumferential, meridian and the thickness directions. Fixed coordinates are along radial and axial directions as shown in Fig.2.3. The radius of the clamped sheet, punch radius and initial thickness of the sheet are denoted by a, R_p, and t_0 respectively. Let at any point of time, the punch travel (cup height) is denoted by H and the corresponding punch force by P. As the sheet is clamped at the outer radius, hence the in-plane displacement of the sheet at the periphery is equal to zero i.e. $u(a) = 0$. Let r_c denotes the radius of the surface element of the sheet at which punch losses its contact with the sheet. The normal to this element makes an angle ϕ_c with the vertical axis, thus punch wraps an angle of $2\phi_c$ in the plane of deformation at a particular instant of time.

A surface element of an axisymmetric shell is taken at a radius r from the center of the sheet which is subtending an angle of $d\theta$ as shown in Fig.2.4. As the thickness of the sheet is small in comparison to radius of punch, the deformation may be assumed to take place under membrane stresses alone, reason being mentioned in the assumptions. The principal stresses acting on the element are σ_θ in the hoop / circumferential direction and σ_ϕ along the meridian direction. The body and inertial forces are neglected since the mode of deformation is assumed to be quasistatic. The normal force per unit surface area applied by the punch is denoted by p and μ is limiting coefficient of friction acting between the punch and sheet surfaces. The frictional force is assumed to follow the Coulomb

14
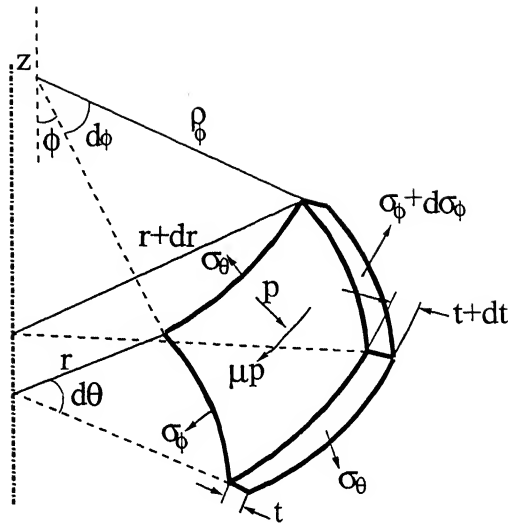
Figure 2.4: *Forces acting on a surface element*

friction law. The variation of stresses across the thickness has also been neglected because such variations are caused by the instantaneous bending of the sheet metal onto the punch surface at early stages of deformation when the strains are small. During plastic deformation of the sheet metal the forces acting on this shell element must remain in equilibrium.

Because the process is axisymmetric both in terms of geometry and loading, the rate of change of variables with respect to θ is zero and hence the equilibrium of forces in the θ or circumferential direction is intrinsically satisfied.

In the normal direction, using the notation shown in Fig 2.4, the equation of equilibrium can be written as

$$(\sigma_\phi + d\sigma_\phi)(r + dr)d\theta(t + dt)\sin\frac{d\phi}{2} + \sigma_\phi r d\theta t \sin\frac{d\phi}{2} + \sigma_\theta \rho_\phi d\phi d\theta \sin\phi$$

$$= p(r + \frac{dr}{2})\rho_\phi d\theta d\phi$$

On simplification and neglecting small terms, the normal equilibrium equation can be obtained as

$$\frac{\sigma_\phi}{\rho_\phi} + \frac{\sigma_\theta}{\rho_\theta} = \frac{p}{t} \tag{2.8}$$

Over a region of contact between the sheet and punch, because of the hemispherical geometry, the two principal radii of curvatures are equal and given by

$$\rho_\phi = \rho_\theta = R_p$$

In view of above, eqn.2.8 becomes

$$\frac{\sigma_\phi + \sigma_\theta}{R_p} = \frac{p}{t} \qquad r \in (0, r_c) \tag{2.9}$$

In the un-supported region, the pressure applied by the punch on the sheet will be zero, therefore eqn.2.8 for this region can be written as

$$\frac{\sigma_\phi}{\rho_\phi} + \frac{\sigma_\theta}{\rho_\theta} = 0 \qquad r \in (r_c, a) \tag{2.10}$$

where ρ_ϕ and ρ_θ are given by eqns.2.6 and 2.7 respectively.

In the meridian direction, the equation of equilibrium can be written as

$$(\sigma_\phi + d\sigma_\phi)(r + dr)(t + dt)d\theta - \sigma_\phi r t d\theta - \sigma_\theta \rho_\phi t d\theta d\phi \cos\phi$$

$$= \mu p r \rho_\phi d\theta d\phi$$

On simplification and neglecting small terms, the above equation can be written as

$$\frac{d(t\sigma_\phi)}{dr} = \frac{t(\sigma_\theta - \sigma_\phi)}{r} + \mu p \sec\phi \tag{2.11}$$

Due to reasons stated for eqns.2.9 and 2.10, eqn.2.11 takes the following forms in contact and non-contact regions

$$\frac{d(t\sigma_\phi)}{dr} = \frac{t(\sigma_\theta - \sigma_\phi)}{r} + \mu p \sec\phi \qquad r \in (0, r_c) \tag{2.12}$$

$$\frac{d(t\sigma_\phi)}{dr} = \frac{t(\sigma_\theta - \sigma_\phi)}{r} \qquad r \in (r_c, a) \tag{2.13}$$

At the contact boundary there is a continuity of meridian forces in between the contact and non-contact regions across the material thickness, thus equating the components of these forces along the direction parallel to the shell axis (refer Fig.2.4), one can get the following equation

$$\sin\phi = \frac{(\sigma_\phi t r)_c \sin\phi_c}{\sigma_\phi t r} \tag{2.14}$$

where terms with subscript c are written for the contact point.

Strain Compatibility Equations

The plastic strains throughout the deformation process must satisfy the compatibility relationship to fulfil continuity. The geometry of the undeformed and deformed element of the shell is shown in Fig.2.5. A line element at a radius s in the initial configuration has attained a current radius r in the deformed configuration and its length has been
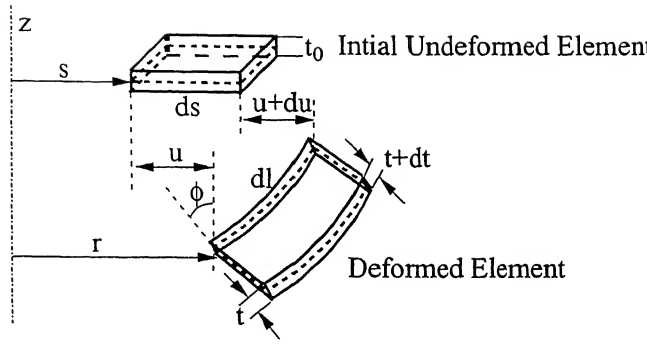
Figure 2.5: *Deformation of the middle surface of shell*

changed from ds to dl in the meridian direction. In plastic deformation, the workpiece undergoes appreciable change in the cross-sectional area. Thus, the strain measured based on the instantaneous dimensions are needed. Therefore, the logarithmic strains are taken in the principal directions which can be expressed as

$$\epsilon_\phi = ln(\frac{dl}{ds}) = ln(\frac{dr}{ds}\frac{1}{\cos\phi}) \; ; \quad \epsilon_\theta = ln\frac{r}{s} \; ; \quad \epsilon_t = ln\frac{t}{t_0} \tag{2.15}$$

respectively. Also the incompressibility condition in plastic deformation can be expressed as

$$\epsilon_\phi + \epsilon_\theta + \epsilon_t = 0 \tag{2.16}$$

From Fig.2.5, it can be noted that

$$r = s + u \implies dr = ds + du \tag{2.17}$$

Substituting eqn.2.17 in expression of ϵ_ϕ in eqn.2.15, yields

$$\frac{du}{dr} = 1 - e^{-\epsilon_\phi}\sec\phi \tag{2.18}$$

Differentiating ϵ_θ in eqn.2.15 with respect to r, one can get

$$\frac{du}{dr} = 1 - e^{-\epsilon_\theta}(1 - r\frac{d\epsilon_\theta}{dr}) \tag{2.19}$$

Equating eqns.2.18 and 2.19 leads to the compatibility condition for the strain components and is obtained as

$$\frac{d\epsilon_\theta}{dr} = \frac{1}{r}(1 - e^{\epsilon_\theta - \epsilon_\phi}\sec\phi) \tag{2.20}$$

Stress Equations

In plane stress state the first two terms of eqn.2.5 can be rearranged as

$$\frac{\epsilon_\phi - \epsilon_\theta}{(1+\bar{R})\sigma_\phi - \bar{R}\sigma_\theta} = \frac{\epsilon_\theta - \epsilon_t}{(2+\bar{R})\sigma_\theta + (1-\bar{R})\sigma_\phi} = \frac{\bar{\epsilon}}{(1+\bar{R})\bar{\sigma}} \qquad (2.21)$$

From eqns.2.21 and 2.16, the following expressions for meridian and circumferential stresses can be obtained

$$\sigma_\phi = -\frac{(1+\bar{R})}{(1+2\bar{R})}\frac{\bar{\sigma}}{\bar{\epsilon}}[\epsilon_\theta + (1+\bar{R})\epsilon_t] \qquad (2.22)$$

$$\sigma_\theta = \frac{(1+\bar{R})}{(1+2\bar{R})}\frac{\bar{\sigma}}{\bar{\epsilon}}[\epsilon_\theta - \bar{R}\epsilon_t] \qquad (2.23)$$

where equivalent strain($\bar{\epsilon}$) and equivalent stress ($\bar{\sigma}$) are given by eqns.2.4 and 2.2 respectively.

Boundary Conditions

As mentioned previously, in hemispherical stretching the sheet is not allowed to move radially inward into the die cavity at the periphery i.e. $r = a$, therefore the in-plane movement of the sheet at this point should be equal to zero i.e.

$$u(t, a) = 0$$

From eqns. 2.15 and 2.17, above condition stated as

$$\epsilon_\theta(t, a) = 0 \qquad (2.24)$$

At the pole ($r = 0$), due to axisymmetric nature of the problem, the state of stresses is that of balanced biaxial tension i.e. $\sigma_\phi = \sigma_\theta$. Therefore by flow rule, we have

$$\epsilon_\phi = \epsilon_\theta \text{ at } r = 0 \qquad (2.25)$$

Punch Load - Punch travel relationship

If z is the vertical height of a generic point on the deformed surface as shown in Fig.2.3, then from geometry

$$\frac{\partial z}{\partial r} = -tan\phi \qquad (2.26)$$

Therefore, once the analysis of a particular stage is completed, the punch travel H at that stage can be calculated by integrating eqn.2.26 as follows

$$H = \sum_{i=1}^{np} z(i) \tag{2.27}$$

where np is the number of elements taken from $r = 0$ to $r = a$ and $z(i)$ is given by

$$z(i) = z(i-1) + 0.5(r(i) - r(i-1))(\tan \phi_{i-1} - \tan \phi_i) \tag{2.28}$$

The punch load at a particular stage is given by the total force in the axial direction exerted by the punch to the sheet at the point of contact. The meridian force per unit length at the point of contact is equal to $(t\sigma_\phi)_c$ where c stands for the contact point and t_c is calculated as

$$t_c = t_o e^{\epsilon_{t_c}}$$

The component of this traction along the direction parallel to shell axis is equal to $(t\sigma_\phi)_c \sin \phi_c$. Thus the total force is calculated as

$$P = 2\pi r_c (t\sigma_\phi)_c \sin \phi_c$$

Putting $r_c = R_p \sin \phi_c$ above equation can be written as

$$P = 2\pi R_p t_c \sigma_c sin^2 \phi_c \tag{2.29}$$

Numerical Procedure

The stresses and strains developed in the deformed region during hemispherical stretching process have been numerically solved by 'initial value technique' and same is described in this section in detail.

The fig.2.6 shows the notations used in this section. At each particular stage, analysis starts at the pole i.e. at $r = 0$ and proceed to the clamped boundary i.e. $r = a$ by assuming a suitable initial value of the circumferential strain $(\epsilon_\theta)_{1,j}$ at the pole, where 1 represents the first point on the deformation region and j stands for the stage of deformation. The initial assumption for the $(\epsilon_\theta)_{1,j}$ is calculated on the basis of the complete analytical solution given by Chakarbarty[6]

Based on the assumption of frictionless and balanced biaxial stress distribution throughout the deformed configuration, Chakrabarty[6] reported the following strain distributions in the contact region:

$$\epsilon_\theta = \epsilon_\phi = \ln \frac{(1 + \cos \phi)(1 + \cos \theta_0)}{(1 + \cos \phi_c)^2} \tag{2.30}$$
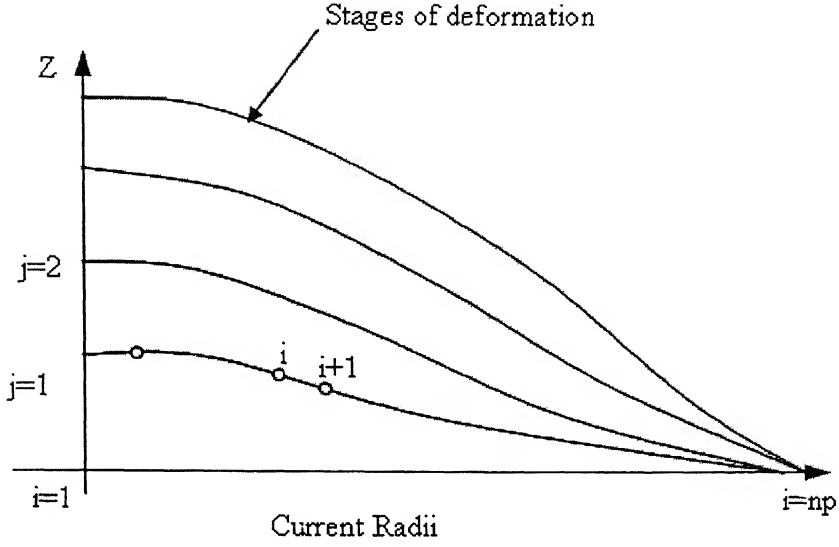
Figure 2.6: *Nomenclature used for the numerical analysis*

where θ_0 is the angle made by the normal to the deformed surface at the clamped periphery with the shell axis and is given by

$$\sin \theta_0 = \frac{R_P}{a} \sin^2 \phi_c$$

Therefore at any stage, the strains at the pole can be obtained by substituting $\phi = 0$ in eqn.2.30 and is given by

$$\epsilon_{\theta 1,j} = \epsilon_{\phi 1,j} = \ln \frac{2(1 + \cos (\theta_0)_j)}{(1 + \cos (\phi_c)_j)^2} \tag{2.31}$$

where the contact angle at stage j is given by

$$(\phi_c)_j = \sin^{-1} \frac{(r_c)_j}{R_p}$$

Equation 2.31 is used to calculate the first approximation of the strain at the pole for starting the analysis at every stage. Using the boundary condition at the pole (eqn.2.25) along with eqn.2.16, the thickness strain value at the pole can be obtained as

$$(\epsilon_t)_{1,j} = -2(\epsilon_\theta)_{1,j}$$

The equivalent strain and stress values can be obtained from eqn.2.4 and eqn.2.2. Using above stress and strain values, the meridian and circumferential stresses can now be obtained from eqns.2.22 and 2.23 respectively. Thus the complete state of principal stresses and strains is now known at the pole for an initial guess value of $\epsilon_{\theta 1,j}$.

Analysis is now carried over to the next point, $r_{i,j}$, in the contact region of the current deformed stage, where all the variables are unknown except $\phi_{i,j}$ which is constrained by the geometry of hemispherical punch. The angle made by the normal at this point with the shell axis is given as

$$\phi_{i,j} = \sin^{-1}\frac{r_{i,j}}{R_p} \qquad (2.32)$$

Analysis at this point starts by assuming an initial value of thickness strain $\epsilon_{ti,j}$. Initial value of circumferential strain $\epsilon_{\theta i,j}$ is then assumed. The meridian strain can thus be obtained from incompressibility as

$$\epsilon_{\phi i,j} = -(\epsilon_{ti,j} + \epsilon_{\theta i,j})$$

The initial guess value of the circumferential strain will be correct only when it satisfies the compatibility equation (eqn.2.20) to maintain the continuity of strain in the deformed region. Thus using calculated values of stress, strains and angle at i^{th} and $(i-1)^{th}$ points for the jth stage, $\epsilon_{\theta i,j}{}'$ can be calculated by the numerical integration of the eqn.2.20 as follows

$$\epsilon_{\theta i,j}{}' = \epsilon_{\theta i-1,j} + 0.5(r_{i,j} - r_{i-1,j})\left[\frac{1}{r_{i,j}}(1 - e^{\epsilon_{\theta i,j} - \epsilon_{\phi i,j}}\sec\phi_{i,j}) + \frac{1}{r_{i-1,j}}(1 - e^{\epsilon_{\theta i-1,j} - \epsilon_{\phi i-1,j}}\sec\phi_{i-1,j})\right]$$

The difference between assumed $\epsilon_{\theta i,j}$ and calculated $\epsilon_{\theta i,j}{}'$ should be negligible for satisfying the compatibility condition.

Therefore $\epsilon_{\theta i,j}$ will be iterated until the above stated difference matches the allowable error limit. The stresses $\sigma_{\phi i,j}$ and $\sigma_{\theta i,j}$ then can be calculated using the eqns.2.22 and 2.23 respectively. The meridian traction in the sheet at the current point $r_{i,j}$ is given by $(t\sigma_\phi)_{i,j}$, where $t_{i,j}$ is calculated using $t_{i,j} = t_0 e^{\epsilon_{ti,j}}$.

Stresses obtained by the plasticity equations should satisfy eqn.2.12 to attain static equilibrium. The initial guessed value of $\epsilon_{ti,j}$ will be correct only when the stresses obtained from it satisfy eqn.2.12. Using the above calculated values of stresses and strains at point $r_{i-1,j}$ and $r_{i,j}$, one can find out $(t\sigma_\phi)_{i,j}{}'$ by numerical integration of eqn.2.12 and is given below

$$(t\sigma_\phi)_{i,j}{}' = (t\sigma_{\phi i-1,j}) + \int_{r_{i-1}}^{r_i}\left[\frac{t(\sigma_\theta - \sigma_\phi)}{r} + \mu p\sec\phi\right]dr$$

where p is given by eqn.2.9. The difference between the meridian traction $(t\sigma_\phi)_{i,j}$ calculated from the assumed thickness strain with that of $(t\sigma_\phi)_{i,j}{}'$ from the equilibrium equation should be negligible for satisfying the static equilibrium. Hence, $\epsilon_{ti,j}$ is iterated until the above stated difference equals the allowable error limit.

Hence the final value of $\epsilon_{ti,j}$ is the one which satisfies the static equilibrium. The stresses and strains is then computed using this value making the analysis at point $r_{i,j}$ complete. The same procedure is repeated for the other points until the contact boundary

is reached.

The deformed profile of the sheet, in non-contact region is unknown. The deformed profile is obtained using vertical equilibrium equation (eqn.2.14) in the non-contact region. Therefore the analysis in this region contains an extra convergence for the angle $\phi_{i,j}$ and is discussed as follows.

Similar to the contact region, the analysis at any point $r_{i,j}$ starts by assuming an initial value for the thickness strain $\epsilon_{ti,j}$. Initial value of circumferential strain $\epsilon_{\theta i,j}$ is then assumed. Now unlike in contact region, the geometry in the non-contact region is unknown, therefore $\phi_{i,j}$ can no longer be calculated using eqn.2.32 and an initial value of $\phi_{i,j}$ has to be guessed to perform the analysis. Therefore, for assumed values of $\epsilon_{ti,j}$, $\epsilon_{\theta i,j}$ and $\phi_{i,j}$, the stresses can be calculated using eqns.2.22 and 2.23. Based on the above calculated stresses, a new value $\phi_{i,j}'$ is calculated using eqn.2.14 as

$$\phi_{i,j}' = \sin^{-1} \frac{(t\sigma_\phi r)_c \sin \phi_c}{(t\sigma_\phi r)_{i,j}}$$

The correct value of $\phi_{i,j}$ for the particular values of $\epsilon_{ti,j}$ and $\epsilon_{\theta i,j}$ is the one for which the difference between $\phi_{i,j}$ and $\phi_{i,j}'$ is negligible and therefore it is iterated until the difference reaches the permissible error limit.

Thus iteration for the above forms the innermost loop in the analysis of non-contact region. The initial guessed value of the circumferential strain $\epsilon_{\theta i,j}$ is then iterated to satisfy the compatibility condition and is done in the same manner as explained in the contact region.

Finally the initial value of the thickness strain assumed in the beginning of the analysis at the current point is then iterated to make the solution to satisfy the static equilibrium. This iteration forms the outermost loop in the analysis and is done similar to the contact region.

The above procedure is continued for other points in the non-contact regions until we reach the clamped boundary i.e. $r_{i,j} = a$.

The whole analysis has been done for an initial guessed value of circumferential strain at the pole, $\epsilon_{\theta 1,j}$, hence circumferential strains calculated may not necessarily satisfy the clamped boundary condition as represented in eqn.2.24. Therefore the whole analysis in contact and non-contact region is iterated for the different values of $\epsilon_{\theta 1,j}$, until the following condition gets satisfied.

$$\epsilon_\theta(np, j) = e$$

where np is the total number of points taken in the deformed region from $r = 0$ to $r = a$ and e is a small value that is used as an allowable error limit at the clamped boundary. It has been found that for particular friction condition, the initial guess of the circumferential strain calculated using eqn.2.31[6] is close to the final converged circumferential

strain at the pole only when the punch travel is less and its value has to be reduced for the fast convergence at higher values of punch travel. Also the above initial guess is found to be close to the converged strain at the pole for the low friction values.

Non-convergence of solution

In the present method, after a certain punch travel the solution was not found to converge at particular point from the pole. It happens when the unit meridian force per unit length $(t\sigma_\phi)$, which is determined on the basis of strain-hardening characteristics and the plasticity theories, cannot attain the value of meridian force per unit length $(t\sigma_\phi)'$ required for satisfying the equilibrium condition at that point. This is defined as the strain propagation instability by Alexander and Kaftanoglu[7] and Woo[5]. Therefore the static equilibrium (eqn.2.11) can never be satisfied for any value of the initial guess chosen for the thickness strain. The initial guess for the circumferential strain$((\epsilon_\theta)_o)$at the pole is then varied in small increments to improve the solution. It has been observed that below certain value of $((\epsilon_\theta)_o)$ the solution converges without satisfying the boundary conditions and above that value, the solution was not converging. Hence the solution which satisfy both the equilibrium as well as boundary conditions cannot be obtained using the present method at this punch travel, due to which the analysis cannot be continued further. The punch travel just prior the occurrence of this condition is taken as the limiting punch height or limiting dome height(LDH).

2.0.3 Formulation for the drawbead analysis

In the present work, drawbead with circular cross-section has been considered for the hemispherical punch stretching of the circular blanks. The geometrical parameters of the drawbead are shown in fig.2.7. A mathematical formulation based on the slab method for calculating the restraining stress at the die opening is presented in this section.

Assumptions

The material related assumptions for the formulation has already been mentioned in the section. Besides those, few more basic assumptions has been used in the formulation and are stated as follows:

- The principal directions are assumed to be in meridian, circumferential and normal directions to the sheet profile.

- The thickness variation in the sheet over the drawbead and the straight flange areas has been neglected.

- The thickness stress is assumed to be negligible over the drawbead and drawbead groove shoulders because the sheet over the drawbead shoulders and the drawbead are in contact with tooling at one surface only[23]. Similarly thickness stress in the unsupported sheet in the clearance region between the drawbead and drawbead groove shoulders is assumed to negligible.

- The plane sections of the sheet is assumed to remain plane and perpendicular to the neutral surface during the bending or unbending of the sheet over the drawbead and drawbead groove shoulders

- The Bauschinger effect is neglected during the cyclic bending and unbending processes.

Geometrical parameters of drawbead

In the present case, an axisymmetric drawbead of circular cross section is considered. Drawbead consists of the semi-circular bead or protrusion on the blank holder surface
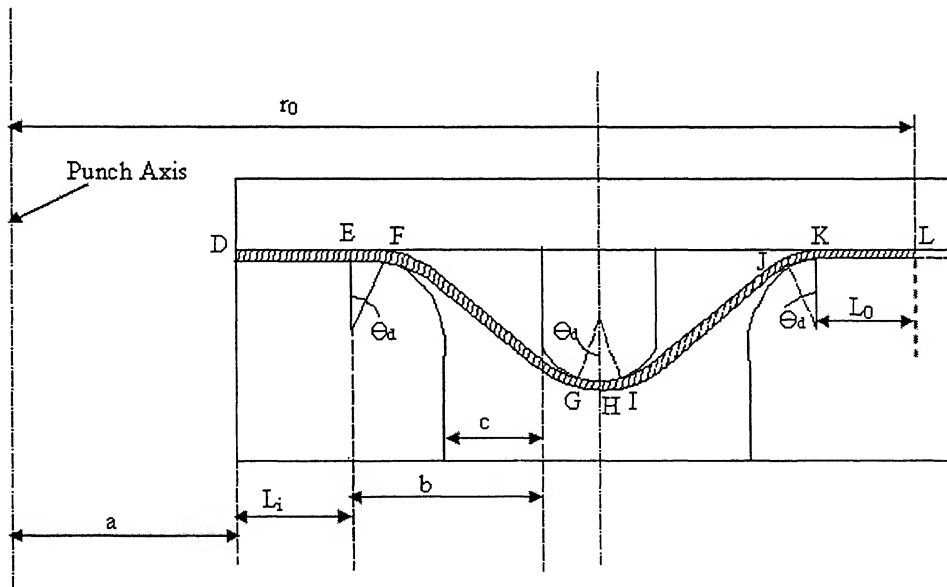

Figure 2.7: *Drawbead Geometrical Parameters*

which fits into the quarter-cylindrical drawbead groove shoulders located on the die surface as shown in the fig.2.7.

The geometrical parameters that can be varied in the considered drawbead are the radius of drawbead (R_d), radius of the drawbead groove shoulder (R_g), height of the drawbead

(H_d) and the radial distance between the centers of the drawbead and drawbead shoulder (b). The clearance between the drawbead and the drawbead groove shoulder (C) can be written as

$$C = b - R_d - R_g$$

The other parameters which will influence the material flow in the flange area are the length of flat flange between die opening edge and the start of the inner drawbead shoulder i.e. region DE as shown in fig.2.7, and length of flat flange between exit of the outer drawbead groove shoulder and the current outer radius r_o of the blank which is equal to

$$L_o = r_o - (a + L_i + 2b)$$

where r_o is calculated from initial blank radius R_o by using the volume constancy.

As shown in fig.2.7, the unsupported regions EF and IJ are assumed to satisfy the tangency condition to the drawbead groove shoulder at point F/J and the drawbead surface at the point J/I. Thus from geometry, sheet will wrap an equal angle θ_d over both the drawbead shoulders. The wrapped region over the drawbead is then equal to $2\theta_d$ which depends on drawbead dimensions viz R_g, R_d, H_d and b.

From fig.2.7, the height of the drawbead for the given value of R_g and R_d can be expressed in terms of θ_d as follows

$$H_d = (R_g + R_d + t_o)(1 - \cos\theta_d - \sin\theta_d \tan\theta_d) + b\tan\theta_d \qquad (2.33)$$

Thus for the given value of H_d, the above transcendental equation can be solved to find out θ_d.

The strain in the meridian direction ϵ_ϕ can be obtained as

$$\epsilon_\phi = \ln\left(\frac{s}{r}\right)$$

where r is current radius of any point in the flange region and s is the initial radius of that point in the undeformed sheet and is calculated by the volume constancy. First the current outer radius of the sheet r_o is calculated as

$$r_o = \sqrt{R_K^2 + R_o^2 - \frac{V}{\pi t_o}} \qquad (2.34)$$

where V is the total volume of the sheet up to the exit of the outer drawbead shoulder i.e. point K (as shown in fig.2.7) whose radius R_K is given as

$$R_K = a + L_i + 2b \qquad (2.35)$$

Now the region between the punch axis i.e. $r = 0$ to outer current radius i.e $r = r_o$ is divided into finite number of points for calculating strains. The initial radius (on initial

blank) of the point corresponding to i_{th} point on the deformed sheet is calculated as

$$s_i = \sqrt{R_o^2 - \frac{V_i}{\pi t_o}} \qquad (2.36)$$

where V_i is the volume of the sheet up to the current point i.e. $r = r_i$ and is calculated from the geometry.

Therefore the strain in the meridian direction at the ith point can be obtained as

$$\epsilon_{\phi i} = \ln\left(\frac{s_i}{r_i}\right) \qquad (2.37)$$

Analysis for calculating the meridian stress at the die opening

The methodology used to calculate the meridian stress at the die opening is to calculate the meridian stress in each region of flange with drawbead which gets developed due to radial drawing and friction. Moreover, the bending stress gets added up due to bending and unbending over drawbead and drawbead groove shoulders. The detailed analysis for the different regions is presented in the following section.

Radial Drawing in the outer flat flange region KL
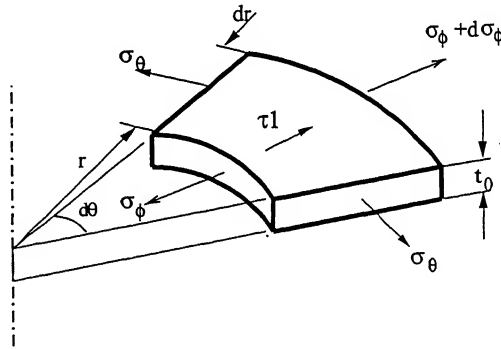
Figure 2.8: *Forces acting on a element in the flat flange region*

Figure2.8 shows the stresses acting on an element in the region KL. Using plane strain condition i.e. $d\epsilon_t = 0$, the relation between σ_ϕ and σ_θ can be obtained from flow rule (eqn.2.5) as

$$\sigma_t = \frac{\sigma_\phi + \sigma_\theta}{2} \qquad (2.38)$$

Using eqn.2.3 and the above relationship, one can get

$$(\sigma_\phi - \sigma_\theta) = \sqrt{\frac{2(1+\bar{R})}{1+2\bar{R}}} \bar{\bar{\sigma}} \qquad (2.39)$$

26

The equivalent strain in plane strain condition can be obtained from eqn.2.4 as

$$\bar{\epsilon} = \sqrt{\frac{2(1+\bar{R})}{1+2\bar{R}}}\,\epsilon_\phi \qquad (2.40)$$

where strain in the meridian direction is given as, $\epsilon_\phi = \ln\left(\frac{s}{r}\right)$, s being the initial radius of the annular element which reaches the radius r after the drawbead is fully clamped and can be calculated as discussed in previous heading.

Substituing eqn.2.40 in the stress strain relationship of material (eqn.2.2), equivalent stress can be written as

$$\bar{\sigma} = K\left[\sqrt{\frac{2(1+\bar{R})}{1+2\bar{R}}}\left(\ln\left(\frac{s}{r}\right)\right)\right]^n \qquad (2.41)$$

The equilibrium equation in the meridian direction for the annular element as shown in fig.2.8 can be written as

$$(\sigma_\phi + d\sigma_\phi)(r+dr)t_o d\theta - \sigma_\phi r d\theta t_o - \sigma_\theta t_o dr d\theta + 2\mu p(r + \frac{dr}{2})dr = 0$$

On simplification and neglecting higher orders terms, above equilibrium equation can be written as

$$\frac{d\sigma_\phi}{dr} = -\left\{\frac{(\sigma_\phi - \sigma_\theta)}{r} + \frac{2\mu p_{bh}}{t_o}\right\} \qquad (2.42)$$

where p_{bh} is the blank holding pressure.

Using eqns.2.39 and 2.41, eqn.2.42 can be written as

$$\frac{d\sigma_\phi}{dr} = -\left[\left\{\sqrt{\frac{2(1+\bar{R})}{1+2\bar{R}}}\right\}^{n+1}\left(\ln\left(\frac{s}{r}\right)\right)^n \frac{K}{r} + \frac{2\mu p_{bh}}{t_o}\right] \qquad (2.43)$$

The stress in the meridian direction at the point K can be obtained by integrating the above equation from $r = r_o$ to $r = R_K$ and is given below

$$\int_{r_o}^{R_K} d\sigma_\phi = -K\left[\left\{\sqrt{\frac{2(1+\bar{R})}{1+2\bar{R}}}\right\}^{n+1}\int_{r_o}^{R_K}\left(\ln\left(\frac{s}{r}\right)\right)^n \frac{dr}{r} + \int_{r_o}^{R_K}\frac{2\mu p_{bh}}{t_o}dr\right]$$

where R_K is given by eqn.2.35.

As the sheet at the outer radius $r = r_o$ is free, the boundary condition for this region is taken as $\sigma_{\phi|r=r_o} = 0$. Using this condition, meridian stress at the entry of the right drawbead shoulder i.e. at point K can be obtained as

$$\sigma_\phi{}^K = K\left[\left\{\sqrt{\frac{2(1+\bar{R})}{1+2\bar{R}}}\right\}^{n+1}\int_{R_K}^{r_o}\left(\ln\left(\frac{s}{r}\right)\right)^n \frac{dr}{r} + \frac{2\mu p_{bh}(R_k - r_o)}{t_o}\right] \qquad (2.44)$$

The integral $\int_{R_K}^{r_o}\left(\ln\left(\frac{s}{r}\right)\right)^n \frac{dr}{r}$ in the above is evaluated using numerical integration.

Analysis in outer drawbead groove shoulder JK

In the region JK, the sheet bends to an effective curvature of $\frac{1}{R_g + \frac{t_o}{2}}$ as it passes the point K and again unbends to a straight unsupported region IJ near the point J where the sheet losses its contact with the outer drawbead shoulder. Thus the sheet will undergoes two fold bending in this region. This causes bending stresses along with radial and frictional stresses. The angle θ_d over which the sheet remain in contact with the outer drawbead shoulder can be obtained using eqn.2.33.
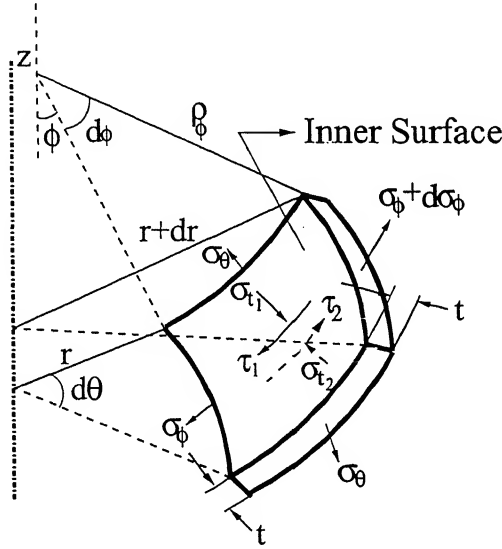

Figure 2.9: *Forces acting on a general volume element*

As mentioned earlier, the sheet is assume to be in plane strain in normal direction due to negligible thickness change and as only one surface of the sheet is in contact with tooling, the thickness stress is assumed to be negligible.

Similar to stretching analysis, forces acting on a shell element is shown in fig.2.9. The stresses with subscript 1 are assumed to act on the inner surface of sheet. The principal radius of curvature in meridian direction is considered as positive if the value of ϕ increases with the increase in value of r.

Using the notation of mentioned fig.2.9, the equilibrium equation in the positive outward normal direction can be written as

$$(\sigma_\phi + d\sigma_\phi)(r + dr)t_o d\theta \sin\frac{d\phi}{2} + \sigma_\phi r t_o d\theta \sin\frac{d\phi}{2} + \sigma_\theta \rho_\phi t_o d\phi d\theta \sin\phi - \sigma_{t1} + \sigma_{t2} = 0$$

On simplification and neglecting higher order terms, above equation can be written as

$$\frac{\sigma_\theta \sin\phi}{r} + \sigma_\phi \cos\phi \frac{d\phi}{dr} + \frac{(\sigma_{t2} - \sigma_{t1})}{t_o} = 0 \tag{2.45}$$

The equilibrium equation in the meridian direction can be written as

$$(\sigma_\phi + d\sigma_\phi)(r + dr)t_o d\theta - \sigma_\phi r t_o d\theta - \sigma_\theta \rho_\phi t_o d\theta d\phi \cos\phi + \tau_2 - \tau_1 = 0$$

on simplification and neglecting higher order terms, equilibrium equation in the meridian equation can be written as

$$\frac{d\sigma_\phi}{dr} + \frac{\sigma_\phi - \sigma_\theta}{r} - \frac{\tau_1 - \tau_2}{t_o \cos\phi} = 0 \qquad (2.46)$$

Equations.2.45 and 2.46 are the general equations of equilibrium and have to be used carefully after identifying the internal and external surfaces of the sheet in different regions. The surface of the sheet which is in contact with the punch is considered as inner surface for reference.

Under the assumption of no thickness variation and negligible thickness stress, the relationship between the stresses in meridian and circumferential direction is as under

$$\sigma_\phi = -\sigma_\theta \qquad (2.47)$$

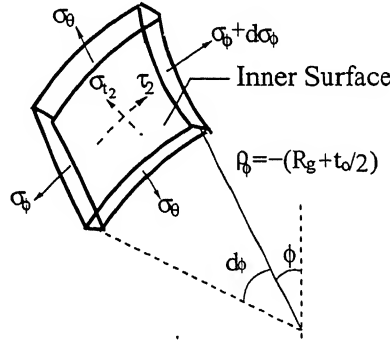In the region JK, the external surface of the sheet is under contact with drawbead

Figure 2.10: *Forces acting on an element over outer drawbead shoulder JK*

shoulder and the forces acting on an element in this region is shown in fig.2.10,from which one can easily write

$$\sigma_{t1} = 0; \quad \sigma_{t2} = \sigma_{t2}; \quad \tau_1 = 0; \quad \tau_2 = \tau_2$$

Using above values along with eqns.2.47 and 2.45 can be expressed as

$$\sigma_{t2} = \sigma_\phi \left\{ \frac{\sin\phi}{r} - \frac{1}{\rho_\phi} \right\} t_o \qquad (2.48)$$

where ρ_ϕ is the principal radius of curvature in the meridian direction and has been replaced for $\frac{1}{\cos\phi}\frac{dr}{d\phi}$.

Similarily the eqn.2.46 can be expressed as

$$\frac{d\sigma_\phi}{dr} + \frac{2\sigma_\phi}{r} + \frac{\tau_2}{t_o \cos\phi} = 0 \tag{2.49}$$

Frictional stress between the drawbead shoulder and sheet is given as $\tau_2 = \mu\sigma_{t2}$. Using the friction condition above equations can be written as

$$\frac{d\sigma_\phi}{dr} = -\left\{\frac{2}{r} + \frac{\mu\tan\phi}{r} - \frac{\mu\sec\phi}{\rho_\phi}\right\}\sigma_\phi \tag{2.50}$$

Using eqns.2.47 and 2.39, one can obtain

$$\sigma_\phi = \frac{1}{2}\sqrt{\frac{2(1+\bar{R})}{1+2\bar{R}}}\,\bar{\sigma} \tag{2.51}$$

Using eqns.2.41 and 2.51, eqn.2.50 can be written as

$$\frac{d\sigma_\phi}{dr} = -\frac{1}{2}\left\{\frac{2}{r} + \frac{\mu\tan\phi}{r} - \frac{\mu\sec\phi}{\rho_\phi}\right\}\left[\sqrt{\frac{2(1+\bar{R})}{1+2\bar{R}}}\right]^{n+1} K\epsilon_\phi{}^n$$

Considering chain rule of differentiation i.e. $\frac{d\sigma_\phi}{d\phi} = \frac{d\sigma_\phi}{dr}\frac{dr}{d\phi}$, above equation can be expressed as

$$\frac{d\sigma_\phi}{d\phi} = -\frac{1}{2}\left\{\frac{2}{r} + \frac{\mu\tan\phi}{r} - \frac{\mu\sec\phi}{\rho_\phi}\right\}\left[\sqrt{\frac{2(1+\bar{R})}{1+2\bar{R}}}\right]^{n+1} K\epsilon_\phi{}^n \frac{dr}{d\phi} \tag{2.52}$$

where $\frac{dr}{d\phi} = \rho_\phi \cos\phi$. For the region JK as shown in fig.2.7, the value of ϕ varies from 0 (at point K) to θ_d (at the point J). Thus the value of ϕ decreases as r increases. Therefore from sign convention stated, principal radius of curvature in meridian direction (ρ_ϕ) is negative and is given by $\rho_\phi = -(R_g + \frac{t_o}{2})$. The radius r in this region can be obtained as

$$r = R_K - (R_g + \frac{t_o}{2})\sin\phi \tag{2.53}$$

Using the above values, eqn.2.52 can be integrated from point K to J as follows

$$\int_0^{\theta_d} d\sigma_\phi = \frac{1}{2}K\left[\sqrt{\frac{2(1+\bar{R})}{1+2\bar{R}}}\right]^{n+1}\int_0^{\theta_d}\left[\left\{\frac{2}{r} + \frac{\mu\tan\phi}{r} + \frac{\mu\sec\phi}{(R_g + \frac{t_o}{2})}\right\}\epsilon_\phi{}^n (R_g + \frac{t_o}{2})\cos\phi\right]d\phi$$

To solve the above equation, the boundary value for σ_ϕ at point K is taken as $\sigma_\phi{}^K$, the meridian stress at point J due to radial drawing and friction, can be obtained as

$$\sigma_\phi{}^J = \sigma_\phi{}^K + \frac{1}{2}K\left[\sqrt{\frac{2(1+\bar{R})}{1+2\bar{R}}}\right]^{n+1}\int_0^{\theta_d}\left[\left\{\frac{2}{r} + \frac{\mu\tan\phi}{r} + \frac{\mu\sec\phi}{R_g + \frac{t_o}{2}}\right\}\epsilon_\phi{}^n (R_g + \frac{t_o}{2})\cos\phi\right]d\phi \tag{2.54}$$

Numerical integration is used to calculate the above integral, where the value of r at every ϕ is calculated using eqn.2.53, the tangential strain ϵ_ϕ is calculated from eqn.2.37 and $\sigma_\phi{}^K$ is given by eqn.2.44.

As the sheet undergoes two fold bending in this region, therefore the central fibre is bent to a curvature of $\frac{1}{R_g + \frac{t_o}{2}}$ at the entrance (point K) of the drawbead shoulder and is unbent again at the exit (point J). The bending stress at the point J can be obtained as[24]

$$\sigma_b = \frac{\overline{\sigma} t_o}{2r_b + t_o} \tag{2.55}$$

where r_b is the bend radius and $\overline{\sigma}$ is the mean value of the flow stress in the region JK. It is calculated using the mean strain between the points K and J as follows,

The meridian strain at the point K is given by

$$\epsilon_K = \epsilon_\phi{}^K$$

where $\epsilon_\phi{}^K$ is calculated using eqn.2.37 at point K.

The strain at the point J will be equal to

$$\epsilon_J = \epsilon_\phi{}^J + \epsilon_b$$

where $\epsilon_\phi{}^J$ is calculated using eqn.2.37 at point J and ϵ_b is the strain due to bending and unbending.

When the straight sheet is bent to a inner fibre radius r_b, then strain associated with bending in the outermost fibre of the sheet can be obtained as

$$\epsilon_s = \frac{t_o}{r_b + \frac{t_o}{2}}$$

Assuming the linear variation of bending strain along the thickness, the average strain in the sheet ϵ_{avg} is equal to $\frac{\epsilon_s}{2}$. Therefore the total strain due to bending and unbending is calculated as

$$\epsilon = 2\epsilon_{avg} = \epsilon_s$$

The corresponding logarithmic strain is given as

$$\epsilon_b = \ln\left(1 + \epsilon_s\right) = \ln\left(1 + \frac{t_o}{r_b + \frac{t_o}{2}}\right) \tag{2.56}$$

Substituting the value of r_b for region JK i.e.$(r_b = R_g)$ in the above equation, one can get ϵ_b at point J as

$$\epsilon_b = \ln\left(1 + \epsilon_s\right) = \ln\left(1 + \frac{t_o}{R_g + \frac{t_o}{2}}\right)$$

Using this value of ϵ_b, the strain at the point J can be obtained as

$$\epsilon_{\phi J} = \epsilon_\phi{}^J + \ln\left(1 + \frac{t_o}{R_g + \frac{t_o}{2}}\right)$$

Mean strain over the outer drawbead shoulder JK is given by

$$\bar{\epsilon}_{JK} = \frac{\epsilon_J + \epsilon_K}{2}$$

The mean flow stress for the region JK can be obtained as

$$\bar{\sigma} = K(\bar{\epsilon}_{JK})^n$$

Using this value, the bending stress $(\sigma_b)_{JK}$ can be calculated using eqn.2.55. Thus the meridian stress at the exit of outer drawbead shoulder is given by

$$\sigma_{\phi tot}{}^J = (\sigma_b)_{JK} + \sigma_\phi{}^K + \frac{1}{2}K\left[\sqrt{\frac{2(1+\bar{R})}{1+2\bar{R}}}\right]^{n+1}\int_0^{\theta_d}\left[\left\{\frac{2}{r}+\frac{\mu\tan\phi}{r}+\frac{\mu\sec\phi}{R_g+\frac{t_o}{2}}\right\}\epsilon_\phi{}^n\left(R_g+\frac{t_o}{2}\right)\cos\phi\right]d\phi$$

$$(2.57)$$

Analysis in the straight unsupported region IJ

The unsupported region IJ is assumed to be tangential to the sheet over the outer drawbead shoulder JK and the drawbead GI at points J and I respectively.
The stress condition in the unsupported region can be written as

$$\sigma_{t1} = 0; \quad \sigma_{t2} = 0; \quad \tau_1 = 0; \quad and \quad \tau_2 = 0$$

Substituting these values in the equilibrium equation in meridian direction (eqn.2.46), it reduces to

$$\frac{d\sigma_\phi}{dr} = -\frac{(\sigma_\phi - \sigma_\theta)}{r}$$

Under the assumption of negligible thickness stress with no variation in thickness, using eqn.2.47, the above equation can be written as

$$\frac{d\sigma_\phi}{dr} = -\frac{2\sigma_\phi}{r} \tag{2.58}$$

Using eqns.2.41 and 2.51, the eqn.2.58 can be written as

$$\frac{d\sigma_\phi}{dr} = -K\left\{\sqrt{\frac{2(1+\bar{R})}{1+2\bar{R}}}\right\}^{n+1}\frac{\epsilon_\phi{}^n}{r} \tag{2.59}$$

Integrating above equation from I to J and using the boundary condition of meridian stress at point J ($\sigma_{\phi|r=R_J} = \sigma_{\phi tot}{}^J$), the tangential stress at the point I can be obtained

as

$$\sigma_\phi{}^I = \sigma_{\phi_{tot}}{}^J + K \left\{ \sqrt{\frac{2(1+\bar{R})}{1+2\bar{R}}} \right\}^{n+1} \int_{R_I}^{R_J} \left\{ \ln\left(\frac{s}{r}\right) \right\}^n \frac{dr}{r} \qquad (2.60)$$

where R_I and R_J are radius of the points I and J respectively and are calculated using following equations

$$R_I = a + L_i + b + \left(R_d + \frac{t_o}{2}\right) \sin\theta_d \qquad (2.61)$$

$$R_J = a + L_i + 2b - \left(R_g + \frac{t_o}{2}\right) \sin\theta_d \qquad (2.62)$$

Analysis over the drawbead region GI

This is the region where the sheet is in contact with the drawbead. The analysis of this region is similar to that of region JK. The sheet undergoes a second sequence of bending
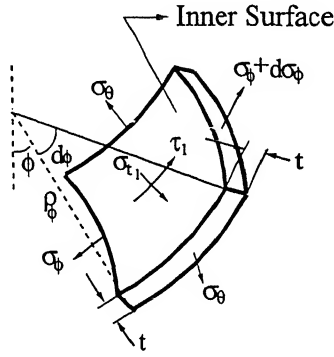

Figure 2.11: *Forces acting on an element over drawbead region GI*

and unbending in this region. A typical element belongs to the region GI with all the stresses acting on it is shown in fig.2.11. The inner surface of the sheet is in contact with the drawbead in this region.

The stresses due to radial drawing have been calcuated separately in two regions HI and GH because the two regions have different principal radii of curvature in meridian direction.

From the fig.2.11, the stress conditions in the region GI can be written as

$$\sigma_{t1} = \sigma_{t1}; \quad \sigma_{t2} = 0; \quad \tau_1 = -\tau_1; \quad \text{and} \quad \tau_2 = 0$$

where τ_1 is the frictional stress between the sheet and drawbead surface and is given as

$$\tau_1 = \mu\sigma_{t1}$$

Substituting above stress conditions in eqns.2.45 and 2.46, equilibrium equations in meridian and normal direction can be respectively expressed as

$$\frac{\sigma_{t1}}{t_o} = \frac{\sigma_\theta \sin \phi}{r} + \sigma_\phi \cos \phi \frac{d\phi}{dr}$$

$$\frac{d\sigma_\phi}{dr} + \frac{\sigma_\phi - \sigma_\theta}{r} - \frac{\tau_1}{t_o \cos \phi} = 0$$

Using the value of τ_1 along with eqn.2.47, the above equations can be expressed as

$$\frac{d\sigma_\phi}{dr} = -\left\{ \frac{2}{r} - \frac{\mu \tan \phi}{r} + \frac{\mu \sec \phi}{\rho_\phi} \right\} \sigma_\phi$$

where ρ_ϕ is the meridian radius of curvature for the region HI and has been replaced for the term $\frac{1}{\cos \phi} \frac{dr}{d\phi}$. Using eqns.2.41 and 2.51, the above equation can be written as

$$\frac{d\sigma_\phi}{d\phi} = -\frac{1}{2}\left\{ \frac{2}{r} - \frac{\mu \tan \phi}{r} + \frac{\mu \sec \phi}{\rho_\phi} \right\} \left[\sqrt{\frac{2(1+\bar{R})}{1+2\bar{R}}} \right]^{n+1} K \epsilon_\phi^n \frac{dr}{d\phi} \qquad (2.63)$$

In the region HI, the value of ϕ varies from 0 (at point H) to θ_d (at point I) i.e., in this region radius r increases as the angle ϕ increases, therefore by used sign convention, principal radius of curvature in the meridian direction is positive and is given by $\rho_\phi = R_d + \frac{t_o}{2}$. The variation of r with respect to ϕ in the region HI is given by

$$r = a + L_i + b + (R_d + \frac{t_o}{2}) \sin \phi \qquad (2.64)$$

Integrating eqn.2.63 from point I to H and using the boundary condition for the tangential stress at point I $(\sigma_{\phi|\phi=\theta_d} = \sigma_\phi^I)$, the meridian stress at the point H due to radial drawing can be obtained as

$$\sigma_\phi^H = \sigma_\phi^I + \frac{1}{2}K \left[\sqrt{\frac{2(1+\bar{R})}{1+2\bar{R}}} \right]^{n+1} \int_0^{\theta_d} \left[\left\{ \frac{2}{r} - \frac{\mu \tan \phi}{r} + \frac{\mu \sec \phi}{R_d + \frac{t}{2}} \right\} \epsilon_\phi^n (R_d + \frac{t_o}{2}) \cos \phi \right] d\phi \qquad (2.65)$$

where r in terms of ϕ is given by eqn.2.64 and σ_ϕ^I is calculated using eqn.2.60.

The region over the second half of the drawbead GH forms the axisymmetric shell with the punch axis. The stress conditions in this region is similar to that in region HI and thus the equilibrium equation (eqn.2.63) would remain valid for the region GH. In this region, the angle made by the normal to the shell (ϕ) varies from 0 at point H to θ_d at point G. Thus the radius (r) of the shell decreases with the increasing value of ϕ. Hence the principal radius of curvature in the meridian direction (ρ_ϕ) is negative according to sign convention and is given as $\rho_\phi = -(R_d + \frac{t_o}{2})$. The value of r in terms of ϕ for this region is given as

$$r = a + L_i + b - (R_d + \frac{t_o}{2}) \sin \phi \qquad (2.66)$$

Differentiating the above term w.r.t ϕ, one can obtain

$$\frac{dr}{d\phi} = -(R_d + \frac{t_o}{2})\cos\phi$$

Integrating eqn.2.63 from point H to point G and using boundary value of meridian stress at point I ($\sigma_{\phi|\phi=0} = \sigma_\phi{}^H$), the tangential stress due to radial drawing at the exit of drawbead (at point G) is given as

$$\sigma_\phi{}^G = \sigma_\phi{}^H + \frac{1}{2}K\left[\sqrt{\frac{2(1+\bar{R})}{1+2\bar{R}}}\right]^{n+1} \int_0^{\theta_d} \left[\left\{\frac{2}{r} - \frac{\mu\tan\phi}{r} - \frac{\mu\sec\phi}{R_d + \frac{t_o}{2}}\right\}\epsilon_\phi{}^n(R_g + \frac{t_o}{2})\cos\phi\right]d\phi \tag{2.67}$$

where r is given by eqn.2.66 and $\sigma_\phi{}^H$ is calculated using eq.2.65.

As mentioned earlier, sheet at the entry of drawbead bends to an effective radius of $(R_d + \frac{t_o}{2})$ and then unbend at the exit of the drawbead i.e. point G to straight unsupported region FG. Therefore the bending stress is calculated similar to the region JK and final expression is given below

$$\sigma_b = \frac{K(\bar{\epsilon}_{GI})^n t_o}{2R_d + t_o}$$

where $\bar{\epsilon}_{GI}$ is the mean strain in the region GI and is given as

$$\bar{\epsilon}_{GI} = \epsilon_\phi{}^G + \epsilon_\phi{}^I + \ln\left(1 + \frac{t_o}{R_d + \frac{t_o}{2}}\right)$$

the strains at points G ($\epsilon_\phi{}^G$) and I ($\epsilon_\phi{}^I$) are calculated using eqn.2.37.

Thus the meridian stress at the exit of the drawbead i.e at point G is given as

$$\sigma_{\phi tot}{}^G = \frac{K(\bar{\epsilon}_{GI})^n t_o}{2R_d + t_o} + \sigma_\phi{}^G \tag{2.68}$$

where $\sigma_\phi{}^G$ is calculated using eqn.2.67.

Analysis in the straight unsupported region FG

Analysis in this region is exactly similar to the region IJ. To solve eqn.2.59 the boundary condition for meridian stress at point G ($\sigma_{\phi|r=R_G}$) is taken as $\sigma_{\phi tot}{}^G$. Hence integrating eqn.2.59 from point G to F, one can obtain the meridian stress at the point F as follows

$$\sigma_\phi{}^F = \sigma_{\phi tot}{}^G + K\left\{\sqrt{\frac{2(1+\bar{R})}{1+2\bar{R}}}\right\}^{n+1} \int_{R_F}^{R_G} \epsilon_\phi{}^n \frac{dr}{r} \tag{2.69}$$

where the tangential strain (ϵ_ϕ) is calculated using eqn.2.37. From fig.2.7 the radius at point G (R_G) and F (R_F) are given by following equations.

$$R_G = a + R_E + b - (Rd + \frac{t_o}{2}) \sin \theta_d \qquad (2.70)$$

$$R_F = a + R_E + (R_g + \frac{t_o}{2}) \sin \theta_d \qquad (2.71)$$

Analysis over the inner drawbead groove shoulder EF

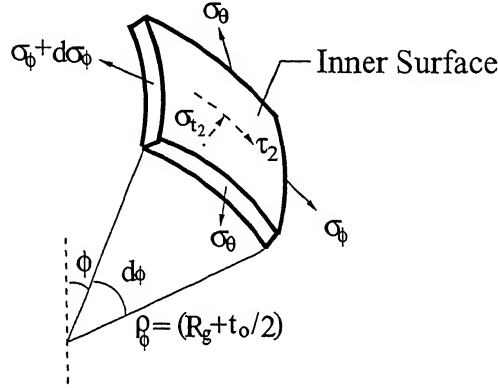The stresses acting on a typical element in the region EF is shown in fig.2.12. The outer

Figure 2.12: *Forces acting on an element inner drawbead shoulder EF*

surface of the sheet is in contact with the drawbead groove shoulder in this region. From fig.2.12, the stress conditions for this region can be written as

$$\sigma_{t1} = 0; \quad \sigma_{t2} = \sigma_{t2}; \quad \tau_1 = 0; \quad \tau_2 = \tau_2$$

which is same as that of region JK. Hence the equilibrium equations derived for the region over the outer drawbead shoulder JK are valid for this region also. In the region EF, angle ϕ made by the normal with the axis parallel to shell axis varies from 0 (at point E) to θ_d (at point F). It indicates that r increases with the increase in the value of ϕ, hence the region EF makes a shell with positive principal radius of curvature in the meridian direction and is given as

$$\rho_\phi = (R_g + \frac{t_o}{2})$$

The combined equation of equilibrium after incorporating the yield criterion (eqn.2.52) is exactly same as that obtained for the region JK and is reproduced here as

$$\frac{d\sigma_\phi}{d\phi} = -\frac{1}{2}\left\{\frac{2}{r} + \frac{\mu\tan\phi}{r} - \frac{\mu\sec\phi}{\rho_\phi}\right\}\left[\sqrt{\frac{2(1+\bar{R})}{1+2\bar{R}}}\right]^{n+1} K\epsilon_\phi{}^n \frac{dr}{d\phi} \qquad (2.72)$$

The value of current radius r in terms of ϕ in the region EF can be written as

$$r = a + L_i + (R_g + \frac{t_o}{2})\sin\phi \qquad (2.73)$$

The boundary condition for the meridian stress (σ_ϕ) is taken as $\sigma_\phi{}^F$ at point F. Integrating eqn.2.72 from point F to point E using above mentioned boundary condition, the meridian stress at the point E due to radial drawing can be obtained as

$$\sigma_\phi{}^E = \sigma_\phi{}^F + \frac{1}{2}K\left[\sqrt{\frac{2(1+\bar{R})}{1+2\bar{R}}}\right]^{n+1}\int_0^{\theta_d}\left[\left\{\frac{2}{r} + \frac{\mu\tan\phi}{r} - \frac{\mu\sec\phi}{R_g + \frac{t_o}{2}}\right\}\epsilon_\phi{}^n(R_g + \frac{t_o}{2})\cos\phi\right]d\phi \qquad (2.74)$$

Over the inner drawbead shoulder EF, the sheet undergoes the third sequence of bending and the unbending. The straight sheet in the region FG bends to an effective radius of $(R_g + \frac{t}{2})$ at the point F and then straightened at the exit of the drawbead shoulder (point E). This adds an extra bending stress and is calculated in similar way as in regions GI and JK.

Thus the meridian stress at the exit of the outer drawbead shoulder is given as

$$\sigma_{\phi tot}{}^E = \frac{K(\bar{\epsilon}_{EF})^n t_o}{2R_g + t_o} + \sigma_\phi{}^E \qquad (2.75)$$

where $\bar{\epsilon}_{EF}$ is the mean strain in the region EF and is calculated as

$$\bar{\epsilon}_{EF} = \epsilon_\phi{}^E + \epsilon_\phi{}^F + \ln\left(1 + \frac{t_o}{R_g + \frac{t_o}{2}}\right)$$

Strains $\epsilon_\phi{}^E$ and $\epsilon_\phi{}^F$ at points E and F respectively are calculated using eqn.2.37.

Analysis in the straight flange region DE

This is the region where the sheet is held between the flat blankholder and die surface. Only the stresses due to radial drawing and friction gets develop in this region. The analysis of this region is similar to the region KL explained earlier.

Equation 2.43 is integrated from point E ($r = R_e$) to point D ($r = a$) as follows

$$\int_{R_e}^a d\sigma_\phi = -K\left[\left\{\sqrt{\frac{2(1+\bar{R})}{1+2\bar{R}}}\right\}^{n+1}\int_{R_e}^a \left(\ln\left(\frac{s}{r}\right)\right)^n\frac{dr}{r} + \int_{R_e}^a \frac{2\mu p_{bh}}{t_0}dr\right]$$

where $Re(= a + R_E)$ is the radius of point E.

The above equation is solved with the following boundary condition at point E

$$\sigma_{\phi|r=R_e} = \sigma_{\phi tot}^{E}$$

Thus the meridian stress at the die opening ($r = a$) is calculated as

$$\sigma_{\phi}^{D} = \sigma_{\phi tot}^{E} + K\left[\left\{\sqrt{\frac{2(1+\bar{R})}{1+2\bar{R}}}\right\}^{n+1} \int_{a}^{R_e} \left(\ln\left(\frac{s}{r}\right)\right)^{n}\frac{dr}{r} + \frac{2\mu p_{bh}(R_e - a)}{t_o}\right] \qquad (2.76)$$

where p_{bh} is the applied blank holder pressure and $\sigma_{\phi tot}^{E}$ is calculated using eqn.2.75

Analysis of flange region is complete once the meridian stress at the die opening σ_{ϕ}^{D} is calculated. The tangential stress σ_{ϕ}^{D} at the die opening is the stress required to pull the sheet into the die opening when the drawbead is in locked position. Hence to restrict the movement of the sheet in die opening during hemispherical stretching, the limiting condition can be expressed as

$$\sigma_{\phi}^{D} = \left(\sigma_{\phi|r=a}\right)_{S} \qquad (2.77)$$

where $\left(\sigma_{\phi|r=a}\right)_{S}$ is the tangential stress developed at the clamped boundary when the full hemispherical bottom is formed or at the inception of instability in the hemispherical stretching.

The parameters that affect the σ_{ϕ}^{D} are R_g, R_d and H_d for the given distance between die opening and inner drawbead groove shoulder (length of region DE), initial outer blank radius R_o, friction coefficient μ, blank holding and pressure p_{bh}.

Chapter 3

Results and Discussions

The problem of designing the drawbead has been decoupled into two steps. In the first step, the stresses in the sheet in the die region are calculated using the formulation presented in section 2.0.2 assuming that the sheet is clamped at the die opening($r = a$). In the second step, the restraining force offered by the drawbead along with the other restraining forces acting on the flange region are calculated using the formulation given in section 2.0.3. The meridian stress at the die opening calculated by the stretching analysis should be smaller than or equal to the stress obtained through the analysis in the flange region.

To validation of the predictions of present model is presented in section 3.1. The effect of various process parameters namely friction coefficient (μ), strain hardening coefficient(n) and the anisotropy value $\overline{R}$ of the material on the strain distributions, punch load and the limiting dome height are presented in section 3.1.1.

3.1 Validation of the stretching analysis

In order to validate the present method, the predictions of the present model (punch load vs punch stroke relation, geometric configuration and thickness strain distribution) have been compared with the results reported by Lee and Yang[2]. They had done the analysis of hemispherical stretching process through energy minimization method and compared the results with those predicted by the rigid plastic finite element method FEM and experimental data reported by Lee et al.[1](source[2]). To validate the model, the required results from the literature have been extracted with the help of digitizer.

Material properties and geometriacal data used for the analysis are same as used by Lee and Yang[2] and are given below

Material: Cold Rolled steel(A)

Material constant,K =601.147MPa

Strain hardening Exponent, n =0.198

Normal anisotropy $\bar{R}$ =1.34

Radius of the punch:R_p =50mm

Radius of the die(radius of the sheet blank):a =60mm

Three lubrication conditions and the corresponding coefficient of friction used are as follows

Low friction condition (teflon-grease lubrication):μ =0.03

Medium friction condition (grease lubrication) :μ =0.12
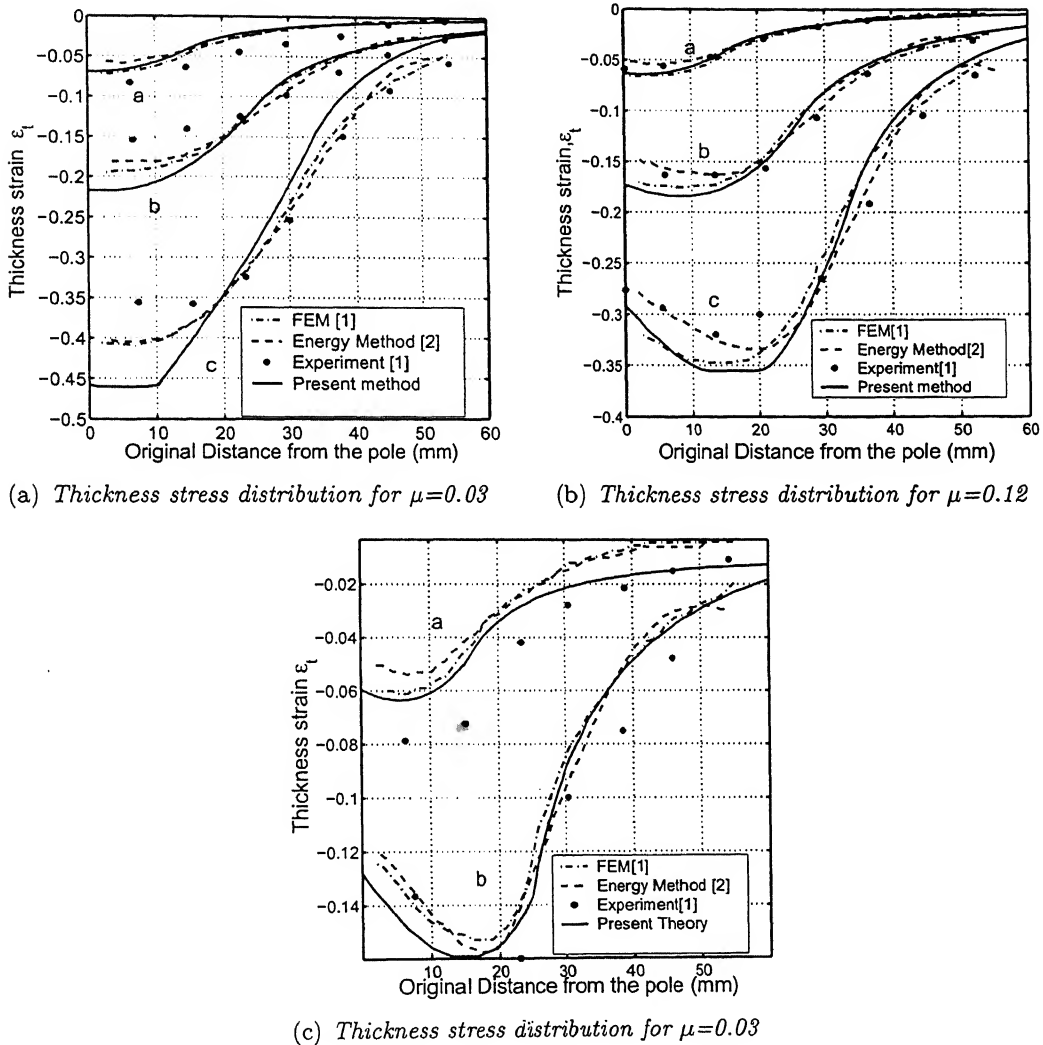
High friction condition (Dry) :μ =0.24

(a) *Thickness stress distribution for μ=0.03*   (b) *Thickness stress distribution for μ=0.12*

(c) *Thickness stress distribution for μ=0.03*

Figure 3.1: *Thickness strain distribution for different friction conditions at the punch travels of a=10mm, b=20mm and c=30mm:Comparison between the present solution and reported results[1];[2]*

Comparison of thickness strain distributions along the radial distance from the pole predicted using the present model are presented in fig.3.1 along with results predicted

by the energy method [2], finite element method and the related experiments[1](source[2]) for different lubrication conditions. The strains in the case of high friction ($\mu = 0.24$) are compared only for the punch travels of 10mm and 20mm (as shown in fig.3.1(c)) because in this case the present method was not-converging after the punch travel of 26.29mm. From fig. 3.1, it can be seen that for all the friction conditions,the obtained thickness strain distributions shows a good agreement with the rigid plastic finite element and the energy method results. The experimental results shows more strain at the clamped boundary in comparisons to the results obtained by the present method. The difference in values are mainly due to the non-consideration of bending effect along the die arc radius in the present work. As the sheet wraps around the punch (for large angles between the loading axis and a deforming element at higher punch travels), the frictional forces retard the movement over the punch. This causes less deformation in the contact region and more in the non-contact regions. Hence the peak value of the strain gradually shift towards the edge of the hemispherical dome with the increase in punch travel.

Fig.3.2 shows the change of the geometric configuration of the sheet and the contact point with the punch travel for medium friction condition ($\mu = 0.12$) for different punch travels. The geometrical configuration of the sheet predicted by the present method is in close agreement with the reported results[[1];[2]]. Figure3.3 shows the comparison
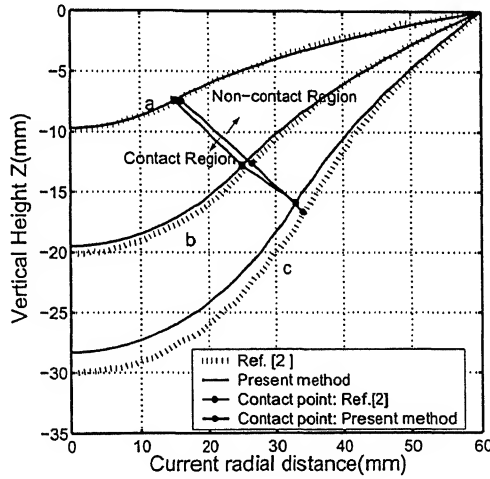

Figure 3.2: *Deformed configurations during hemispherical punch stretching when the punch strokes are: a=10mm, b=20mm and c=30mm : Comparison between the present solution and reported results[2]*

of punch load vs stroke relationship predicted using the present method with that of reported results[[1];[2]] for different friction conditions. For all the friction conditions, the predictions of the present method shows good agreement with those by the finite element method[1](source[2]) and the energy method[2]. In addition, it can be seen from fig.3.3 that the predicted results are in good agreement with the experimental results reported[1](source[2]])
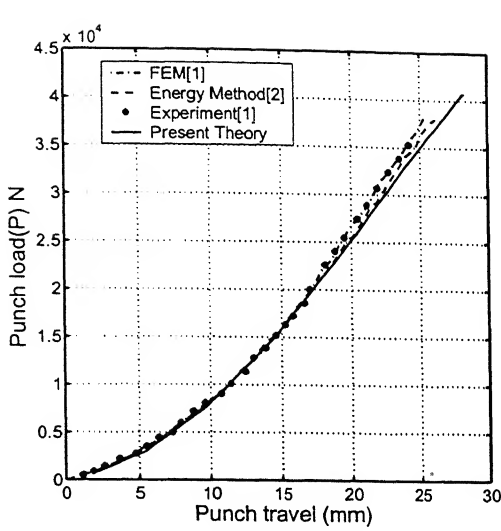
(a) *Punch load vs stroke diagram for μ=0.03*
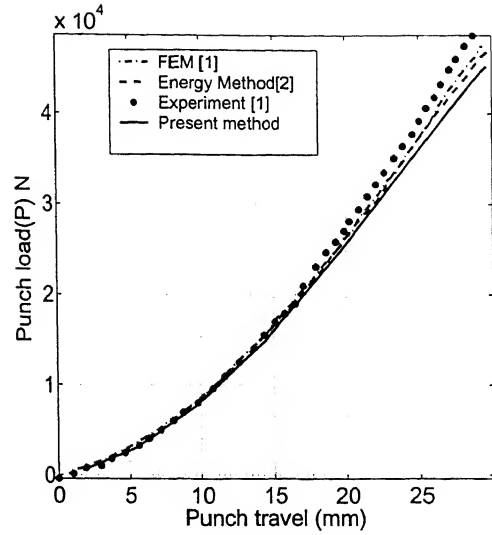
(b) *Punch load vs stroke diagram for μ=0.12*
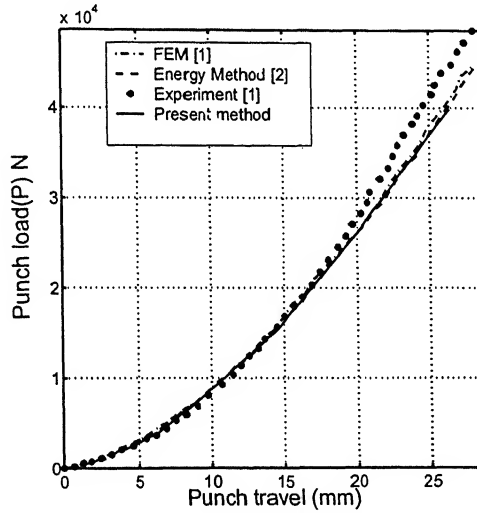
(c) *Punch load vs stroke diagram for μ=0.24*

Figure 3.3: *Punch Load vs stroke diagrams for different friction conditons:Comparison between the present solution and reported results[1];[2]*

The limiting dome height that can be achieved in hemispherical punch stretching with the present model has been compared with the results reported by Yang and Hsu[3]. The material and geometrical parameters used for the analysis are taken from the Yang and Hsu[3] and are reproduced below

Material: Mild steel(**B**)

Material constant,K =581.8Mpa

Radius of the punch:R_p =50mm

Radius of the die(radius of the sheet blank):a =54mm

The variation of limiting dome height predicted using the present method for varying friction coefficient(μ), strain hardening coefficient(n) and normal anisotropy ratio(R) is
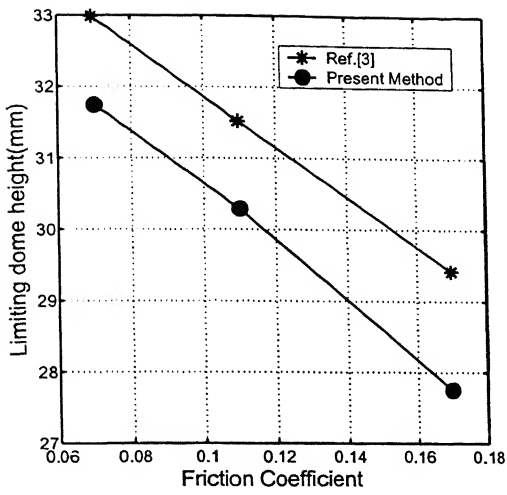
(a) *Limiting dome height for different friction conditions with $\overline{R} = 1.78$ and $\mu = 0.132$*
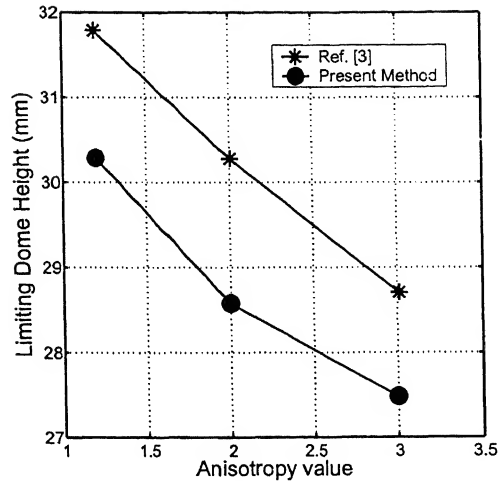
(b) *Limiting dome height for different anisotropy values with $n = 0.258$ and $\mu = 0.312$*
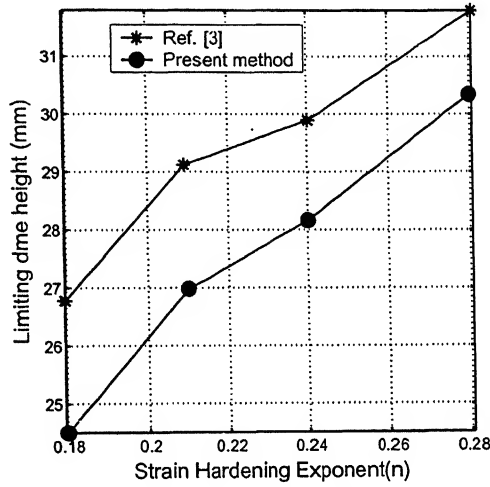
(c) *Limiting dome height for different strain hardening(n)coefficient values with $\overline{R} = 1.78$ and $\mu = 0.132$*

Figure 3.4: *Comparison of limiting dome height predicted by using present method with the results reported [3]*

shown in fig.3.4 along with the results reported by Yang and Hsu[3]. It can be seen that the results predicted by the present model at are in reasonably good agreement with the results reported[3] with a maximum error of ± 9%. In addition the variation of limiting dome height with the varying material properties follows the same trend as reported by Yang and Hsu[3].

3.1.1   Parametric Study

The important process parameters that influence the stretching process are friction condition (μ) between the sheet and the punch, strain hardening coefficient(n) and the anisotropy value ($\overline{R}$) of the sheet material. In this section the effect of these parameters on the strains distribution, punch load and limiting dome height is presented.

Effect of varying friction coefficient

The effect of friction on the strain distribution in the hemispherical stretching of the material A is shown in fig.3.5 for different punch travels. The thickness strain distribution for different friction conditions at the punch travels of 10mm and 20mm are shown in fig.3.5(a) The increase in the friction retards the movement of the material over the
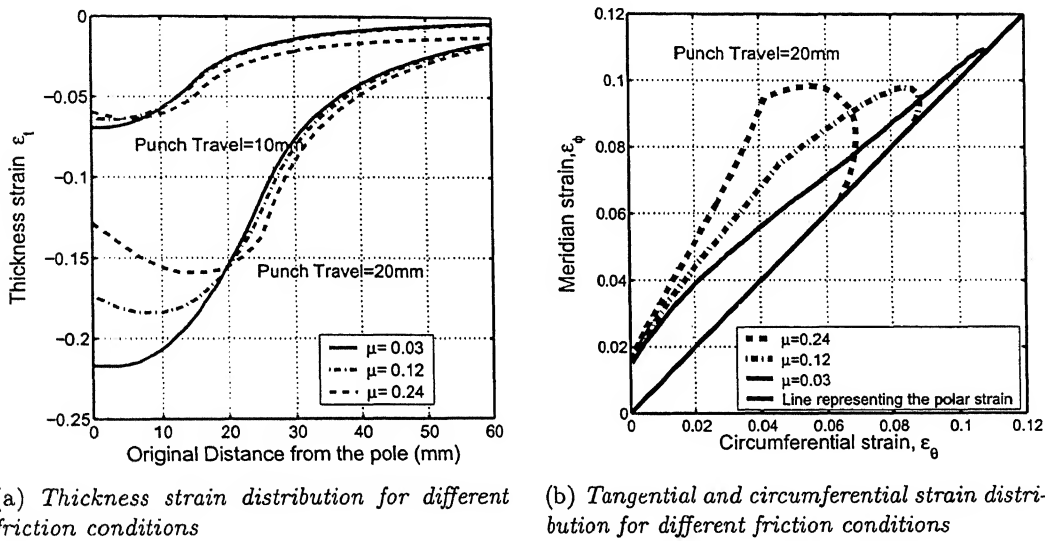

(a) *Thickness strain distribution for different friction conditions*

(b) *Tangential and circumferential strain distribution for different friction conditions*

Figure 3.5: *Strain distribution in the hemispherical stretching of material A for different friction conditions*

punch. Thus for a given punch travel, the higher friction produces less thinning in contact region while more thinning is observed in the unsupported region. This causes the strain peak to gradually shift towards the edge of the hemispherical dome. It can also be noticed that the effect of friction on the thickness strain distribution in the deformed region is not significant at low punch travels and it increases with the increase in punch travel.

The effect of friction condition on the tangential and circumferential strains in the deformed region is shown in fig.3.5(b) for punch travel of 20mm. The line at 45° angle with the axes shows the state of strain at pole as both the tangential and radial strain are equal on it. Similarly, the axis point on the ϵ_ϕ represent the strain state at the clamped boundary. It can be seen that the with the increase in friction the peak value of the
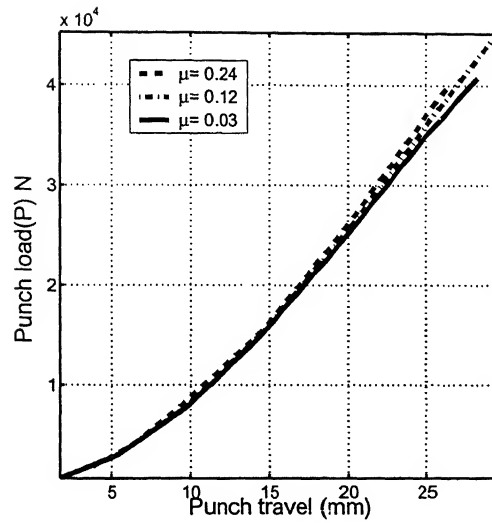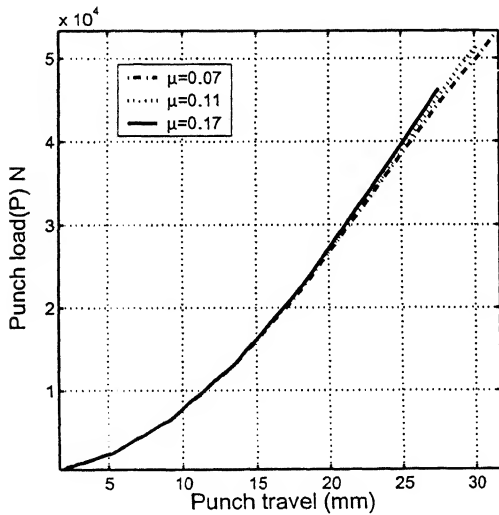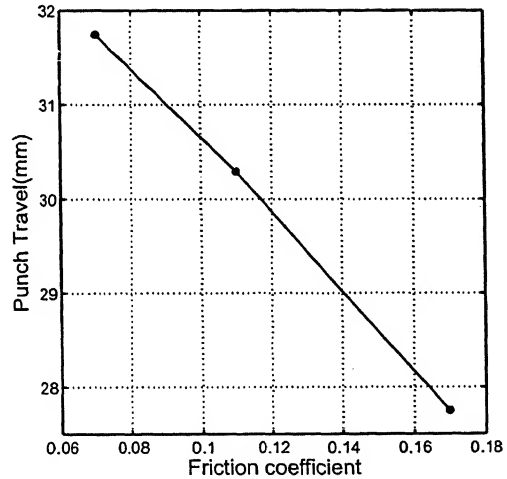
Figure 3.6: *Effect of friction on the punch travel in the hemispherical punch stretching of material A[2]*

(a) *Punch load vs punch travel relationship for different friction conditions*

(b) *Limiting dome height for different friction conditions*

Figure 3.7: *Punch Load and limiting dome height in the hemispherical punch stretching of material B for friction conditions with $\overline{R} = 1.78$ and $\mu = 0.132$*

tangential strain increases and it shifts towards the edge of hemispherical dome. From above discussion it is evident that increase in friction over the punch results in more non-uniform distribution of strains in the deformed region.

Fig.3.6 shows the punch travel predicted at the different friction materials in the hemispherical punch stretching of the material A. It can be seen that the high friction results in high punch load. The same trend is also shown in fig.3.7(a). which shows the punch load calculated at the different friction condition. High friction results in lower limiting punch travel as shown in fig.3.7(b) because it produces more non-uniform distribution

of strain over the contact region which increases the chances of localized thinning in the deformed region. It can also be seen that the peak value of strain moves away from the punch with increasing friction.

Effect of normal anisotropy ($\overline{R}$)

The resistance of the material towards thinning increases with the increase in normal anisotropy($\overline{R}$). Therefore the increase of normal anisotropy results in decreases of thickness strains in the contact region as shown in fig.3.8(b). The distribution of strains in the deformed region also become more non-uniform with the high normal anisotropy value as shown in figs.3.8(a) and 3.8(b). Increase in $\overline{R}$ value increases the punch load

(a) Meridian strain distribution for different anisotropy values

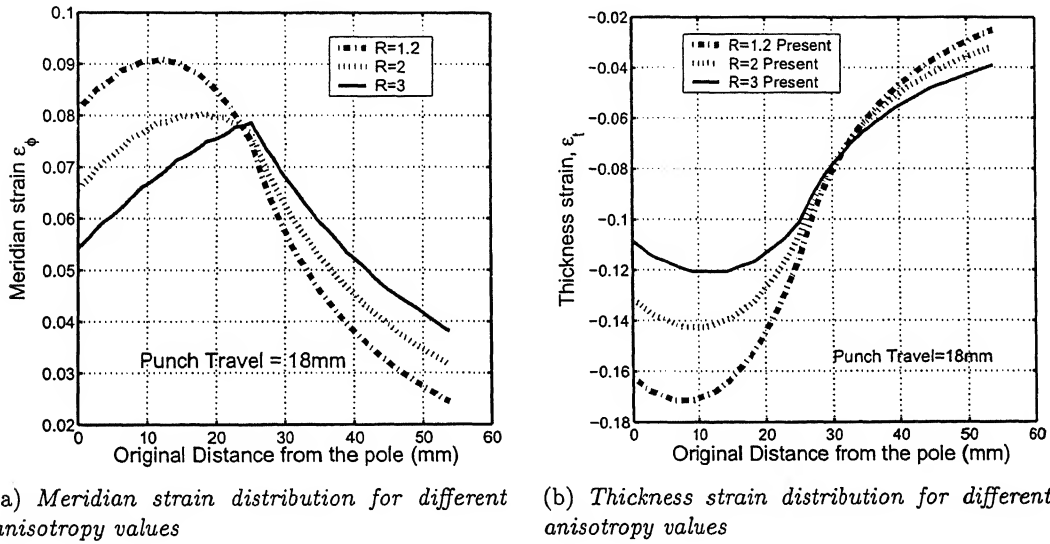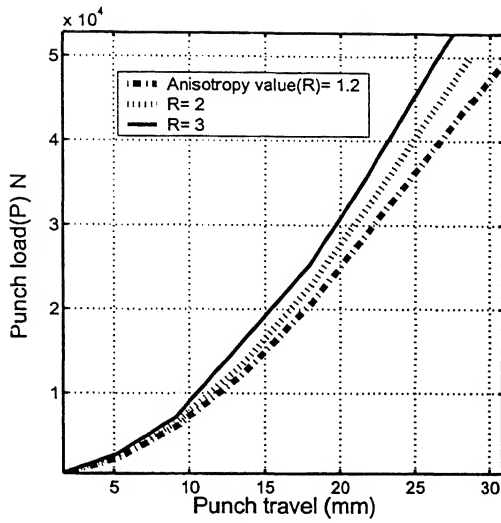(b) Thickness strain distribution for different anisotropy values

Figure 3.8: Strain distribution in the hemispherical punch stretching of material B for different anisotropy values with $n = 0.258$ and $\mu = 0.132$

requirement as shown in fig.3.9(a). It is because the increase in $\overline{R}$ value increases resistance of the material towards the thinning and hence more load is required to stretch the material at a particular punch travel. The variation of limiting dome height(LDH) for the different $\overline{R}$ values is shown in fig.3.9(b). Increase in normal anisotropy decreases the limiting dome height due to increased non-uniform distribution of strains in the deformed region.

Effect of strain hardening exponent(n)

The effect of varying strain hardening exponent(n) on the strain distributions is shown in fig.3.10. With the increase in the strain hardening exponent(n), the material get more hardened when strained. Therefore the most highly strained region gets most hardened
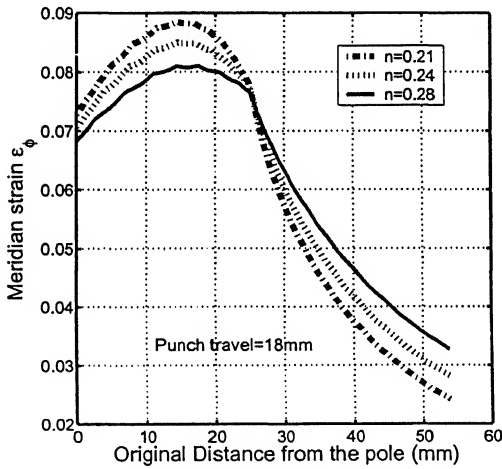
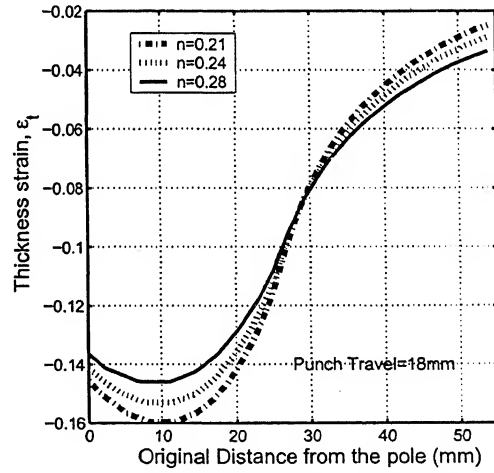(a) *Punch load vs punch travel relationship for different anisotropy values*
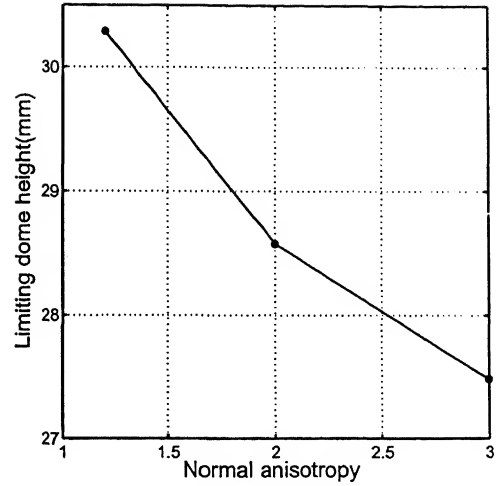
(b) *Limiting dome height for different anisotropy values*

Figure 3.9: *Punch load and limiting dome height in the hemispherical punch stretching of material B for different anisotropy values with $n = 0.258$ and $\mu = 0.132$*
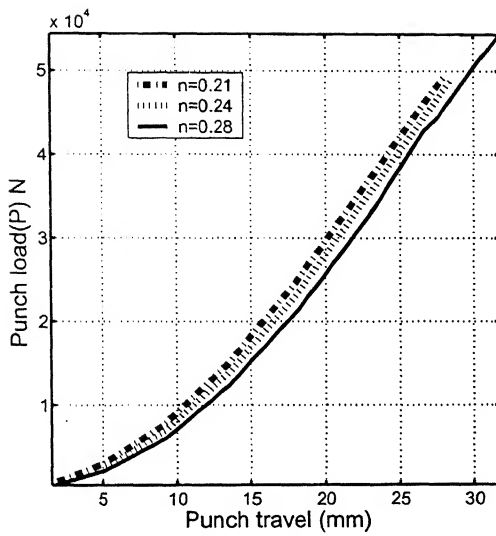

(a) *Meridian strain distribution for different strain hardening exponent*
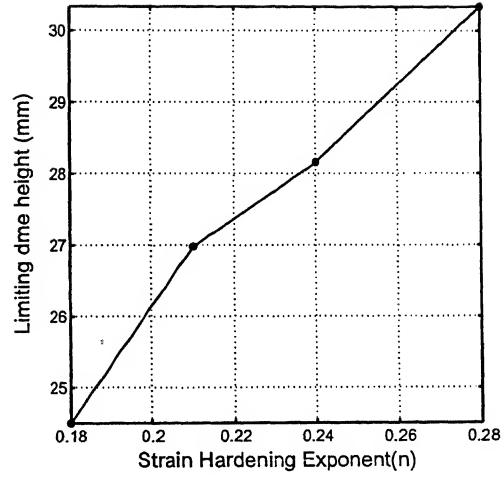
(b) *Thickness strain distribution for different strain hardening exponent*

Figure 3.10: *Strain distribution in the hemispherical punch stretching of material B for different strain hardening exponent values with $\overline{R} = 1.78$ and $\mu = 0.132$*

and the load is passed on to the neighboring elements. This causes mores straining in those elements and in result, the strain gradient gets reduced. Hence high strain hardening coefficient value gives more uniform distribution of strains in the deformed region. This is shown in fig.3.10 where the tangential and thickness strain distributions get more uniformly distributed with the increase in n value. Due to above reasons the increased value of n also results in less thinning in the supported region as shown in fig.3.10(b). Figure 3.11(a) shows that the punch load requirement decreases with the increase in strain hardening coefficient because of more uniform deformation at high

47

(a) *Punch load vs punch travel relationship for different strain hardening exponent*

(b) *Limiting dome height for different strain hardening(n)exponent*

Figure 3.11: *Punch load and limiting dome height in the hemispherical punch stretching of material B for different strain hardening(n)coefficient values with $\overline{R} = 1.78$ and $\mu = 0.132$*

value of n. The high value of strain hardening coefficient increases the limiting dome height as shown in fig.3.11(b) because high value of n results in high limit strains at which the material fails and secondly it gives more uniform distribution of strain in the deformed region.

Thus it can be inferred from the above discussion that the friction, anisotropy and strain hardening coefficient have a significant influence on the strain distribution, limiting dome height and punch load.

3.2 Parametric study for the drawbead analysis

In the present work the blank holder with a circular drawbead of semi-circular cross section has been taken into consideration. The presence of drawbead in the blank holder increases the flow restriction in the flange region. It is because the sheet metal would have to bend around the bead as it is being pulled through the flange region.

The restraining stress($\sigma_\phi{}^D$) at the die opening is calculated when the drawbead is fully locked with the corresponding groove shoulder on the die surface. The fully locked drawbead condition is defined as the stage when the clearance between the blank holder and die surface is equal to the thickness of the sheet. This condition is shown in fig.2.7. Drawbead restraining force is caused to a large extent from the bending and unbending of the sheet metal over the drawbead region. Therefore the parameters that affect the developed stress ($\sigma_\phi{}^D$) are the radius of the drawbead(R_d), height of the drawbead(H_d)

48

and the radius of the groove shoulder(R_g). The other parameters which will affect the radial stress at die opening are length of outer(L_o) and inner(L_i) flat flange, blank holding pressure(p_{bh}) and the friction (μ) between the sheet and tooling(die and blank holder surfaces). The length of outer flat flange depends on the initial blank radius(R_o) of the sheet. The parametric study for the effect of drawbead geometry parameters (R_d, R_g and H_d) on the the restraining stress (σ_ϕ^D) is presented in this section.

The material A is used for the drawbead analysis. The geometrical parameters used are given below

Geometrical parameters: Radius of the punch,R_p =50mm

Radius of the die opening,a =60mm

Initial thickness of the sheet,t_o =0.8mm

Initial blank radius,R_o =95mm

Length of inner flat flange,L_e=5mm

The blank holder pressure (p_{bh}) is assumed to be constant. The general range of the blank holding pressure that is used in the deep drawing process is 2-10N/mm^2[24]. For the present work, the blank holding pressure is assumed to be constant and its value is taken as $4N/mm^2$.

Each of the three drawbead geometry parameters (R_d, R_g and H_d) are varied separately keeping the other two parameters constant to study their affect on the restraining stress developed at die opening (σ_ϕ^D).

Effect of drawbead height(H_d)
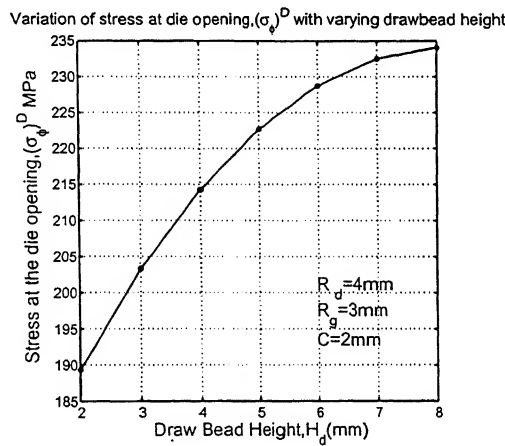

Figure 3.12: *Variation of stress at the die opening (σ_ϕ^D) with different drawbead height (H_d)*

Fig.3.12 shows the relation between the restraining stress developed at the die opening(σ_ϕ^D) with the drawbead height(H_d). It can be seen that the σ_ϕ^D increases with the increase in drawbead height The reason that can be attributed to this is that with the

increase in H_d the radial drawing increases which results in more restraining stress at the die opening. In addition, with the increase in drawbead height, the covering angle(θ_d) over which the sheet comes in contact over the drawbead increases. As a result, the bending and unbending stress around the drawbead and drawbead shoulders increases which leads to the increase in restraining stress $\sigma_\phi{}^D$.

Effect of radius of the drawbead(R_d) and drawbead groove shoulder(R_g)
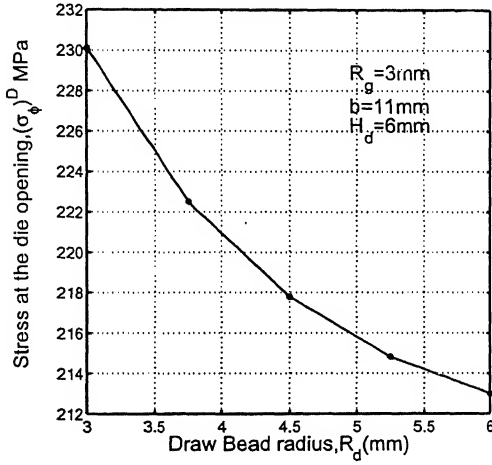

Figure 3.13: Variation of stress at the die opening ($\sigma_\phi{}^D$) for different radius of drawbead (R_d)
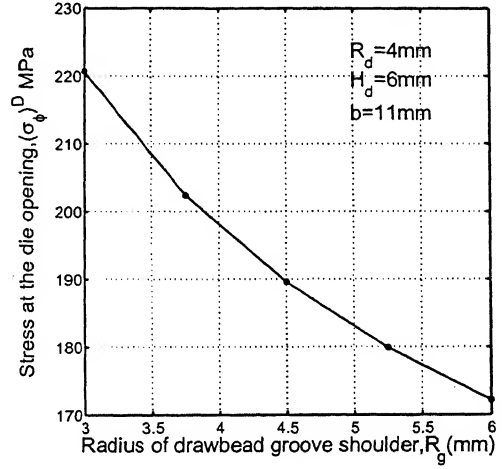
Figure 3.14: Variation of stress at the die opening ($\sigma_\phi{}^D$) for different radius of drawbead groovw shoulder(R_g)

Figs.3.13 and 3.14 shows variation of meridian stress at the die opening ($\sigma_\phi{}^D$) with the radius of drawbead and drawbead groove shoulder. The bending and unbending stress in the bend sheet is inversely proportional to the radius of curvature of bend. Therefore increase in radius of drawbead and drawbead groove shoulder decreases the bending and unbending stress over them which leads to the increase in the meridian stress at the die opening ($\sigma_\phi{}^D$). Hence the resistance of the sheet against the radial drawing in flange region increases with the decrease in R_d and R_g.

Effect of clearance C

The clearance(C) between the drawbead and the drawbead groove shoulder is varied by varying the width of drawbead groove opening(b) for a constant value of R_d and R_g and is then given as

$$C = b - R_d - R_g$$

The relation between the stress developed at the die opening and the clearance C is shown in fig.3.16. The stress at the die opening decreases with the increase in C value.
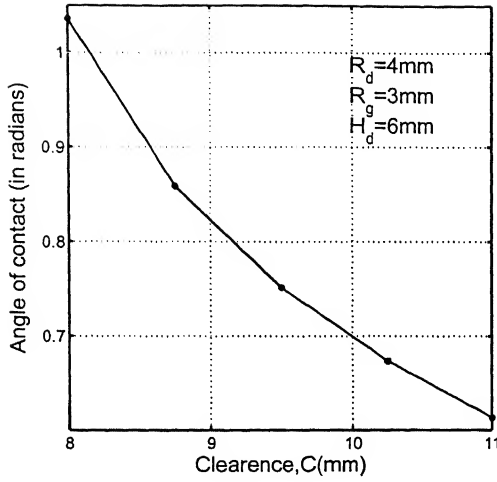
Figure 3.15: Angle of contact(θ_d) for different values values of clearance(C) between drawbead and the drawbead groove shoulder
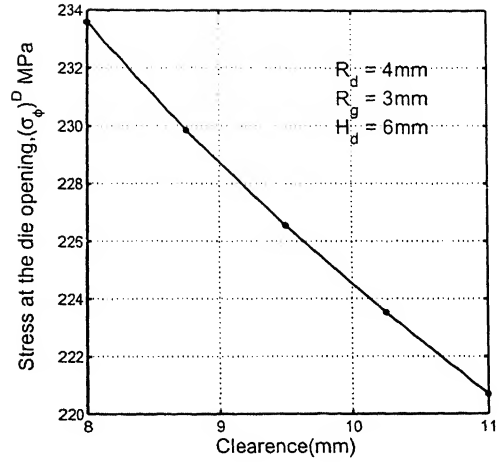
Figure 3.16: Stress at the die opening $(\sigma_\phi{}^D)$ for different values of clearance(C) between drawbead and the drawbead groove shoulder

The reason for this is that with the increase in C value, the angle of contact(θ_d) of the sheet over the drawbead and the drawbead shoulder decreases as shown in fig.3.15. Thus the bending and unbending stresses over the drawbead and the drawbead groove shoulder decreases with the decrease in clearance (C). In addition for the other fixed parameters, increase in C value decreases the outer flat flange length which in turn reduces the radial and friction stresses over it.

It can be clearly noticed from the above parametric study that the drawbead height, radius of drawbead and drawbead groove shoulder and clearance significantly influence the resistance stress against the flow of material in the flange region. Thus the optimum value of these parameters has to be evaluated for the proper designing od drawbead for the hemispherical stretching process keeping in mind the boundary condition(eqn.3.1) i.e.

$$\sigma_\phi{}^D = \left(\sigma_{\phi|r=a}\right)_S \tag{3.1}$$

required for restraining the material at the die opening

Chapter 4

Conclusion and Scope of Future work

4.0.1 Conclusion

The following conclusions are drawn from the present work:

- The process of hemispherical stretching is analyzed using the developed method based on principle of force equilibrium and total strain theory. The results predicted are in good agreement with the results reported in literature.[[1];[2];[3]].

- The predicted strain distributions, deformed geometry and punch load are found to be in good agreement with the reported results [[1];[2]]. The predicted limiting dome height is found to be in reasonably good agreement with the reported result[3] with a maximum error of $\pm 9\%$. .

- The effect of process parameters namely strain hardening exponent (n), normal anisotropy (R) and the friction coefficient(μ) on the process are studied. Following observations are made on the influence of these parameters on strain distribution, limiting dome height and punch travel

  - A larger value of the strain hardening exponent(n) will results in more uniform strain distribution in the deformed region, a increased limiting dome height and a reduced punch load.

  - A larger value of the anisotropy parameter$(\overline{R})$ results in more non-uniform distribution, reduced limiting dome height and high punch load.

  - A higher friction coefficient(μ) will results in more non-uniform strain distribution in the deformed region, reduced limiting dome height and high punch load.

- An analytical model has been developed based on the slab method for the analysis of flow of material over the drawbeads with circular cross section for axisymmetric hemispherical punch stretching process.

- The restraining stress at the die opening is calculated using the developed model. The drawbead geometry parameters namely radius of drawbead (R_d), radius of drawbead groove shoulder(R_g), height of drawbead(H_d) and clearance(C) are found to significantly influence the developed restraining stress at the die opening. A larger value of H_d, smaller values of R_d and R_g and a smaller value of C will results into high restraining stress at the die opening.

4.0.2 Scope for the future work

Further work can be planned to consider the following aspects

- The optimum parameters of the drawbead can be determined for the hemispherical punch stretching of circular blanks .

- An instability analysis can be carried out to find the more accurate limiting dome height so that an effective boundary condition for the stress at the die opening can be developed for better optimization model.

- The model developed for calculating the restraining force can be extended for the condition once the material start moving into the die cavity.

References

[1] H. B. Shim, C. H. Lee and D. Y. Yang. Determination of friction coefficient for sheet metal working and its application to stretch forming. *Proceedings of the 6th International Congress on Experimental Mechanics and Manufacturers Exhibit, Portland Oregon*, pages 71–76, 1988.

[2] H. S. Lee and D. Y. Tang. An analysis of hemispherical punch stretching ny the energy method. *International Journal Of Mechanical Sciences*, 33(6):435–447, 1991.

[3] T. S. Yang and T. C. Hsu. Forming limit analysis of hemispherical-punch stretching. *Journal of Material Processing Technology*, 117:32–36, 2001.

[4] M. Samuel. Influence of drawbead geometry on sheet metal forming. *Journal of Material Processing Technology*, 122:94–103, 2002.

[5] D.M.Woo. The stretch forming test. *The Engineer*, 220, Nov 1965.

[6] J. Chakarbarty. A theory of stretch forming over hemispherical punch heads. *International Journal of Mechanical Sciences*, 12(315):315–325, 1970.

[7] B. Kaftanoglu and J. M. Alexander. On quasistatic axisymmetrical stretch forming. *International Journal of Mechanical Sciences*, 12:1065–1084, 1970.

[8] D. Banabic. Analysis of punch-stretching in vibratory regime. *Journal of Materials Processing Technology*, 60:201–204, 1996.

[9] A. S. Wifi. An incremental complete solution of the stretch-forming and deep-drawing of a circular blank using a hemispherical punch. *International Journal of Mechanical Sciences*, 18:23–31, 1976.

[10] S. I. Oh, J. H. Kim and S. Kobayashi. Analysis of stretching of sheet metals with hemispherical punch. *International Journal of Mechanical Sciences*, 18:209–226, 1978.

[11] Tze-Chi Hsu and Chan-Hung Chu. A finite element analysis of sheet metal forming processes. *Journal of Material Processing Technology*, 54:70–75, 1995.

[12] T. Yoshida, T. Katayama and M. Usada. Forming-limit analysis of hemispherical-punch stretching using the three-dimensional finite-element method. *Journal of Material Processing Technology*, 50:226–237, 1995.

[13] H. D. Nine. New drawbead concept for sheet metal forming. *Journal Of Applied Metal Working*, 2:185–192, 1982.

[14] F. K. Chen and P. C. Tszeng. An analysis of drawbead restraining force in the stamping process. *International Journal Of Machine Tools and Manufacture*, 38:827–842, 1998.

[15] C. Weidemann. The blank holder action of drawbeads. *in:Proceedings of the 10th Biennial IDDRG Congress*, pages 79–85, 1978.

[16] Li Shuhui, Lin Zhongqin, Xu Weili and Bao Youxia. An improved equivalent drawbead model and its application. *Journal of Material Processing Technology*, 121:308–312, 2002.

[17] L. R. Sanchez and K. J. Wienmann. An analytical and experimental study of the flow of sheet metal between circular drawbeads. *Journal of Engineering for Indusiry*, 118:45–53, 1996.

[18] N. Triantafyllidis, B. Maker and S. K. Samanta. An analysis of drawbeads in sheet metal forming:part1-problem formulatiom. *Journal of Engineering Materials and Technology*, 108:321–327, 1986.

[19] Y. Y. Yang, Z. H. Jin, R. F. Wang and Y. Z. Wang. 2D elasto-plastic FE simulation of the drawbead drawing process. *Journal of Material Processing Technology*, 120:17–20, 2002.

[20] T. Meinders, B. D. Carleer, H. J. M. Geijselaers and J. Huetink. The implementation of an equivalent drawbead model in a finite-element code for sheet metal forming. *Journal of Material Processing Technology*, 83:234–244, 1998.

[21] Y. T. Keum, B. Y. Ghoo and J. H. Kim. Application of an expert drawbead model to the finite element simulation of sheet forming process. *Journal of Material Processing Technology*, 111:155–158, 2001.

[22] H. L. Cao and C. Teodosiu. Numerical simulation of drawbeads for axisymmetric deep-drawing. *Numerical Methods in Industrial Forming Processes*, pages 439–448, 1992.

[23] T. Z. Blazynski. *Plasticity and modern metal-forming technology*. Elsevier Science Publishers Ltd., Essex IG11 8JU, England, 1989.

[24] Kurt Lange, editor. *Handbook of Metal Forming*. McGraw-Hill Book Company, 1985.

[25] J. L. Duncan Z. Marciniak and S. J. Hu. *Mechanics of sheet metal forming*. Butterworth Heinemann, Woburn, MA, second edition, 2002.

[26] R. Hill. The mathematical theory of plasticity. *Clarendon Press, Oxford(U.K.)*, 1950.